IMMUNOLOGY

PRKAG2.2 is essential for FoxA1$^+$ regulatory T cell differentiation and metabolic rewiring distinct from FoxP3$^+$ regulatory T cells

Sara Mandatori[1], Yawei Liu[1], Joana Marturia-Navarro[1], Mahdieh Hadi[1], Kristine Henriksen[1], Jin Zheng[1], Louise Munk Rasmussen[1], Salvatore Rizza[2], Klaus H. Kaestner[3], Shohreh Issazadeh-Navikas[1]*

Forkhead box A1 (FoxA1)$^+$ regulatory T cells (T_{regs}) exhibit distinct characteristics from FoxP3$^+$ T_{regs} while equally effective in exerting anti-inflammatory properties. The role of FoxP3$^+$ T_{regs} in vivo has been challenged, motivating a better understanding of other T_{regs} in modulating hyperactive immune responses. FoxA1$^+$ T_{regs} are generated on activation of the transcription factor FoxA1 by interferon-β (IFNβ), an anti-inflammatory cytokine. T cell activation, expansion, and function hinge on metabolic adaptability. We demonstrated that IFNβ promotes a metabolic rearrangement of FoxA1$^+$ T_{regs} by enhancing oxidative phosphorylation and mitochondria clearance by mitophagy. In response to IFNβ, FoxA1 induces a specific transcription variant of adenosine 5′-monophosphate–activated protein kinase (AMPK) γ2 subunit, PRKAG2.2. This leads to the activation of AMPK signaling, thereby enhancing mitochondrial respiration and mitophagy by ULK1-BNIP3. This IFNβ-FoxA1-PRKAG2.2-BNIP3 axis is pivotal for their suppressive function. The involvement of PRKAG2.2 in FoxA1$^+$ T_{reg}, not FoxP3$^+$ T_{reg} differentiation, underscores the metabolic differences between T_{reg} populations and suggests potential therapeutic targets for autoimmune diseases.

INTRODUCTION

Regulatory T cells (T_{regs}) are demonstrated to be essential for maintaining peripheral tolerance in the body (*1*, *2*). T_{regs} are defined by expression of CD4$^+$CD25^{high} and constitutively express forkhead box P3 (FoxP3) transcription factor (*3*), a "master controller" of their development and function (*4*, *5*) and referred as FoxP3$^+$ T_{regs}. The role of transforming growth factor–β (TGFβ) has been extensively studied in shaping and differentiating FoxP3$^+$ T_{regs} (*6*). Both in humans and mice, CD4$^+$CD25^{high} T_{regs} account for approximately 5 to 10% of peripheral CD4$^+$T cells in the blood, and they play a vital role in maintaining immunologic self-tolerance by actively suppressing self-reactive lymphocytes (*1*, *2*). Depletion of CD4$^+$CD25^{high} T_{regs} in rodents results in spontaneous development of multiple organ-specific and systemic autoimmune diseases and promoting antitumor immune responses. Conversely, reconstitution of T_{reg} prevents autoimmune diseases (*2*, *7*, *8*).

It is reported that FoxP3 expression and the fate of FoxP3$^+$ T_{regs} might not be consistently stable in vivo (*9*). Moreover, it is probable that different tissues require distinct T_{regs} to fulfill their functions, as previously indicated (*10*). This is further influenced by various insults and immune activation, which necessitate the immune system to establish mechanisms that safeguard tissue integrity while allowing for adaptable and variable immune responses. These factors highlight the importance of comprehending the characteristics of additional T_{regs} that exhibit suppressive and anti-inflammatory responses.

Forkhead box A1 (FoxA1)$^+$ T_{regs} are a distinct subset of T_{regs} that are induced by the antiviral cytokine interferon-β (IFNβ) and hold a suppressive function by inhibition of proliferation and induction of apoptosis in autoreactive T cells (*10*). FoxA1$^+$ T_{regs} are associated with positive response to IFNβ treatment of patients with multiple sclerosis (MS), inflicted with an autoimmune disease affecting the central nervous system (*10*). In addition, the suppressive function of FoxA1$^+$ T_{regs} plays a role in lung cancer by limiting lung-infiltrating T cells′ proliferation and promoting tumor growth (*11*). We previously reported that FoxA1$^+$ T_{regs} have a distinct transcriptional profile, characterized by FoxA1 transcription factor expression that induces the programmed cell death ligand 1 (PD-L1) (*12*) allowing induced FoxA1$^+$ T_{regs} (iFoxA1$^+$ T_{regs}) to suppress skin and central nervous system inflammation (*10*). However, the complete understanding of mechanisms through which FoxA1$^+$ T_{regs} are generated by IFNβ is unknown.

It is known that metabolism of T cells plays an important role in driving and promoting their activation, expansion, and differentiation. It has been shown that naïve T cells are metabolically quiescent and rapidly rewire metabolic networks upon cytokine stimulation to expand and differentiate in T cell subsets (*13*–*15*). Among CD4$^+$ T cells, T helper cells rely on glycolysis for their function and differentiation, which is the pathway that uses glucose to generate adenosine triphosphate (ATP) and the reduced form of nicotinamide adenine dinucleotide (NADH) (*16*, *17*). Differently, FoxP3$^+$ T_{regs} reprogram their metabolism enhancing oxidative phosphorylation (OXPHOS) to support their suppressive function (*18*–*20*). It has been shown that T cell metabolism can be modulated by adenosine 5′-monophosphate (AMP)–activated protein kinase (AMPK) (*21*), a pivotal kinase promoting the development of regulatory and anti-inflammatory T cells while limiting the generation of inflammatory T cells (*13*, *22*). AMPK is composed of one catalytic

[1]Neuroinflammation Unit, Biotech Research and Innovation Centre, Faculty of Health and Medical Sciences, University of Copenhagen, Copenhagen, Denmark. [2]Redox Biology Group, Danish Cancer Society Research Center, Copenhagen, Denmark. [3]Department of Genetics, University of Pennsylvania School of Medicine, Philadelphia, PA, USA.
*Corresponding author. Email: shohreh.issazadeh@bric.ku.dk

(α) and two regulatory (β and γ) subunits that associate to form a heterotrimeric (*23*). Each α and β subunit is encoded by two genes (α1 and α2 or β1 and β2), whereas the γ subunit is encoded by three genes (γ1, γ2, and γ3) (*24*). γ1 and γ2 are the main isoforms expressed in T cells (www.proteinatlas.org). The subunit γ has a noncatalytic function, although it provides AMPK its ability to sensitively detect shifts in AMP, adenosine 5′-diphosphate (ADP), and ATP levels (*25*). To date, the studies investigating the relationship between type I IFN cytokine stimulation and metabolic rewiring in T cells are sparse. It is known that type I IFNs are potent pleiotropic cytokines that broadly alter cellular functions, including metabolic programs such as fatty acid oxidation and OXPHOS in plasmacytoid dendritic cells (pDCs) and nonhematopoietic cells (*26*). We also recently revealed IFNβ's role in regulating mitochondrial fission and OXPHOS pathway in neurons (*27*–*29*). The role of IFNβ signaling in the metabolic regulation of FoxA1$^+$ T$_{regs}$ remains unclear, and its influence on their fate determination has not been established. In this study, our objective is to investigate how IFNβ signaling affects mitochondrial homeostasis and the specific metabolic mechanisms that drive the differentiation of FoxA1$^+$ T$_{regs}$ and determine their fate.

RESULTS

IFNβ regulates mitochondrial homeostasis in iFoxA1$^+$ T$_{regs}$

Given the fact that type 1 IFNs (IFNα and IFNβ) affect cellular metabolism in pDCs (*26*) and IFNβ treatment reprograms both naïve and bulk CD4$^+$ T cells (human and mouse) into suppressive FoxA1$^+$ T$_{regs}$ (*10*), we first investigated the metabolic signature driven by IFNβ during FoxA1$^+$ T$_{reg}$ differentiation. To generate in vitro IFNβ-induced FoxA1$^+$ T$_{regs}$ (hereby iFoxA1$^+$ T$_{reg}$ conditions), human naïve CD4$^+$ T cells were isolated from healthy donors and cultured with/without human recombinant IFNβ (hIFNβ). RNA sequencing (RNA-seq) and transcriptomic analysis were performed on iFoxA1$^+$ T$_{regs}$ in comparison to naïve CD4$^+$ T cells (fig. S1A). For identifying the main metabolic pathways regulated under iFoxA1$^+$ T$_{reg}$ conditions, we selected metabolic gene sets from the Molecular Signatures Database and applied Gene Set Enrichment Analysis (GSEA), a widely used knowledge-based approach to interpreting genome-wide expression profiles (Fig. 1A) (*30*). Compared to the untreated naïve CD4$^+$ T cells, 93.75% of metabolic gene sets were up-regulated, and 6.25% were down-regulated uniquely in iFoxA1$^+$ T$_{regs}$ (Fig. 1B).

The top up-regulated gene sets of iFoxA1$^+$ T$_{regs}$ were related to mitochondrial respiration, mitochondria physiology, and mitochondria homeostasis (Fig. 1, C to G). To functionally validate the transcriptomic analysis, we assessed in vitro experiments by isolating bulk CD4$^+$ T cells from wild-type (WT) mice, which are numerically more consistent than naïve CD4$^+$ T cells, and we still can induce FoxA1$^+$ T$_{reg}$ differentiation. CD4$^+$ T cells were treated with anti-CD3 and anti-CD28 to induce T cell activation (*31*, *32*) and with IFNβ to generate iFoxA1$^+$ T$_{regs}$ (iFoxA1$^+$ T$_{reg}$ conditions) (fig. S1B). The bioenergetic profile of iFoxA1$^+$ T$_{regs}$, measured by oxygen consumption rate (OCR) as the rate of basal OXPHOS, was elevated under iFoxA1$^+$ T$_{reg}$ conditions with comparison to CD4$^+$ T cells (Fig. 1, H and I), indicating the involvement of OXPHOS during FoxA1$^+$ T$_{reg}$ differentiation. OXPHOS is the driving force behind ATP production led by electron transport and mitochondrial transmembrane proton pumping (*33*, *34*). To better investigate the biology of mitochondria under iFoxA1$^+$ T$_{reg}$ conditions, mitochondrial transmembrane potential (ΔΨm) and mitochondrial mass were quantified by tetramethylrhodamine ethyl ester (TMRE) and MitoTracker Green (MTG), respectively. We detected a significant mitochondrial mass reduction and mitochondrial transmembrane potential increase under iFoxA1$^+$ T$_{reg}$ conditions (Fig. 1, J and K). In line with the reduction of mitochondrial mass, we also found a decrease in electron transport chain protein levels under iFoxA1$^+$ T$_{reg}$ conditions (fig. S1C), suggesting either a decrease in mitochondrial biogenesis or an increase in mitochondrial turnover, presumably by mitophagy (*35*).

To address a potential involvement of mitochondrial biogenesis in the reduction of mitochondrial mass, we evaluated the DNA mitochondria D-loop region by quantitative polymerase chain reaction (qPCR) and observed no changes under iFoxA1$^+$ T$_{reg}$ conditions compared to CD4$^+$ T cells (fig. S1D). Next, we performed live imaging of mitochondria (MTG) and lysosomes [LysoTracker Red (LTR)] to address the mitophagy rate under iFoxA1$^+$ T$_{reg}$ conditions versus CD4$^+$ T cells. We found a significant increase in mitochondria-lysosome colocalization in iFoxA1$^+$ T$_{regs}$, similar to the positive control [carbonyl cyanide 3-chlorophenylhydrazone (CCCP) treatment, a mitophagy inducer] (Fig. 1, L and M), supporting mitophagy induction upon IFNβ signaling. During mitophagy, damaged mitochondria are engulfed into vesicles that are coated with the autophagosome marker Microtubule-associated proteins 1A/1B (MAP1) light chain 3B (LC3B) (*36*). A lipidated form of LC3B, LC3B-II, has been shown to be an autophagosomal marker (*37*); thus, we checked the accumulation of LC3B-II in iFoxA1$^+$ T$_{regs}$, upon treatment with the lysosomal acidification inhibitor bafilomycin (Baf) (*38*). Fluorescence-activated cell sorting (FACS) and Western blot (WB) data confirm that autophagic flux was induced during iFoxA1$^+$ T$_{reg}$ differentiation (Fig. 1N), presumably to sustain mitophagy rate. The engulfment of mitochondria into autophagosome is guided by adaptor proteins such as p62 connecting LC3 with the cargo. FACS analysis of p62 upon lysosome inhibition shows only a mild increase in this adaptor protein (fig. S1, E and F), suggesting that mitophagy in iFoxA1$^+$ T$_{regs}$ relies on different adaptors.

FoxA1 transcription factor is required for mitochondrial respiration and mitophagy during FoxA1$^+$ T$_{reg}$ differentiation

As FoxA1 is a lineage factor of FoxA1$^+$ T$_{regs}$ (*10*), activation of which depends on IFNβ, we investigated whether FoxA1 affected FoxA1$^+$ T$_{reg}$ mitochondrial homeostasis. We established a mouse strain of Foxa1$^{flox/flox}$ backcrossed with CD4^{cre} mice, in which FoxA1 expression is absent in T cells (fig. S1, G and H). CD4$^+$ T cells were isolated from CD4^{Cre} and CD4^{Cre}Foxa1$^{fl/fl}$ mice and were cultured under iFoxA1$^+$ T$_{reg}$ conditions. As expected, there was no detection of iFoxA1$^+$ T$_{reg}$ from CD4^{Cre}Foxa1$^{fl/fl}$ mice versus CD4^{Cre} mice (Fig. 2, A and B, and fig. S1I). We next analyzed the basal mitochondrial metabolism profile by Seahorse. We found significantly lower mitochondrial respiration under iFoxA1$^+$ T$_{reg}$ conditions from CD4^{Cre}Foxa1$^{fl/fl}$ mice versus CD4^{Cre} mice (Fig. 2, C and D), suggesting that FoxA1 might sustain mitochondrial respiratory activity. To further validate this discovery, we conducted a Seahorse analysis comparing WT with *Ifnar1*$^{-/-}$ T cells, which lack the interferon-alpha/beta receptor alpha chain (IFNAR) receptor 1 and consequently do not generate FoxA1$^+$ T$_{regs}$ (*10*, *12*). Consistent with

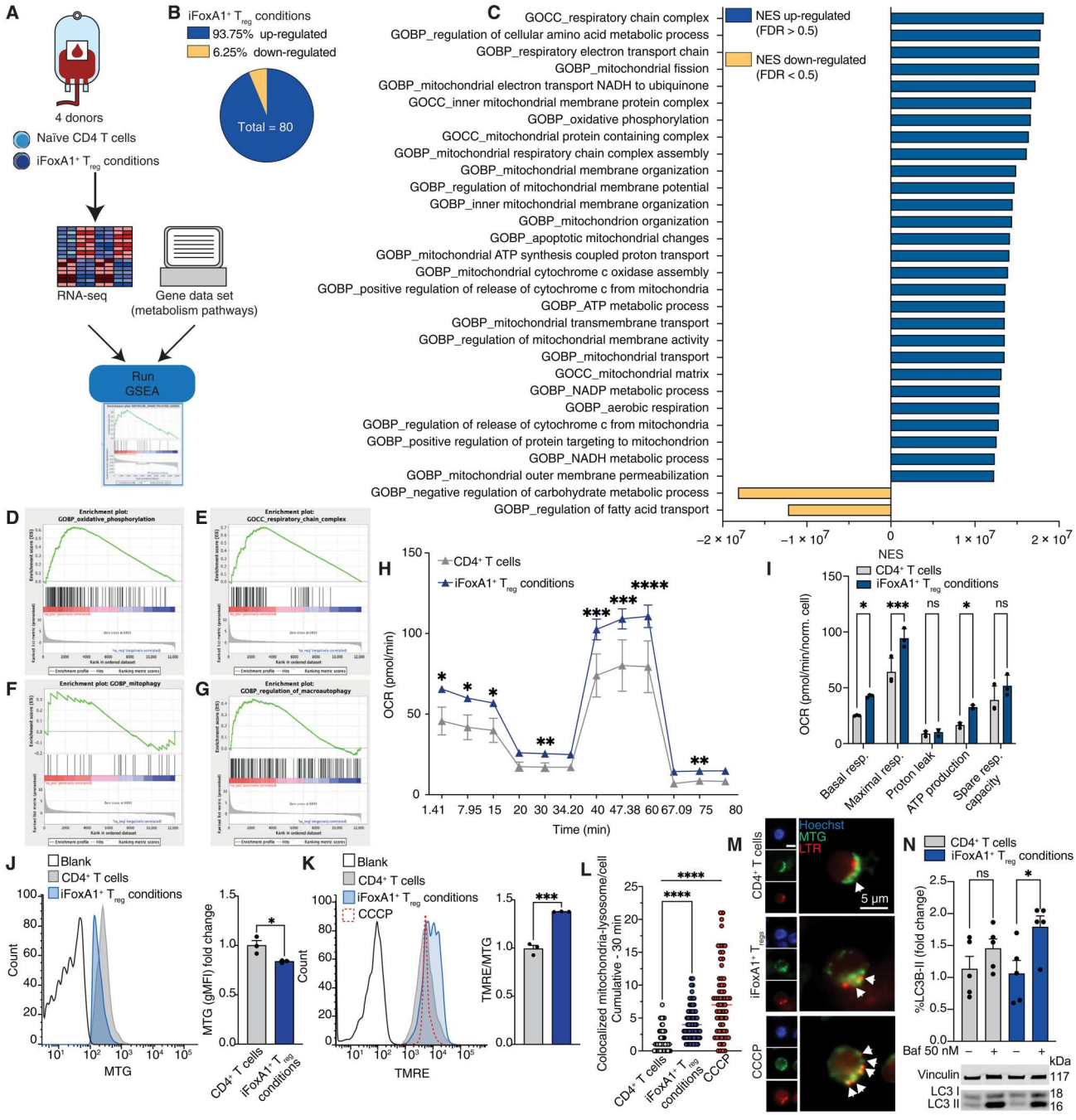

Fig. 1. IFNβ regulates mitochondrial homeostasis in iFoxA1$^+$ T$_{regs}$. In all experiments, CD4$^+$ T cells were treated with IFNβ for 24 hours/48 hours to induce FoxA1$^+$ T$_{regs}$ (iFoxA1$^+$ T$_{reg}$ conditions or iFoxA1$^+$ T$_{regs}$). (**A**) Schematic drawing of GSEA analysis. (**B**) Pie chart of RNA-seq data in human CD4$^+$ T cells versus iFoxA1$^+$ T$_{regs}$ [GSEA analysis and Gene Ontology (GO) gene sets]. (**C**) GO Biological Processes (GOBP) and GO Cellular Components (GOCC) up-regulated [false discovery rate (FDR) > 0.5] and down-regulated (FDR < 0.5) gene sets were analyzed as in (B), represented as normalized enrichment score (NES). (**D** to **G**) GSEA plots. Green line, cumulative enrichment score; black lines, gene ranking in the GSEA pathway; red and blue gradients, positive and negative regulation; gray, visualizes ranking metric scores. The boxed genes are the leading-edge subsets, contributing significantly to the enrichment score. (**H** and **I**) Seahorse analysis of oxygen consumption rate (OCR) on CD4$^+$ T cells and iFoxA1$^+$ T$_{regs}$ obtained from three WT mice (five to seven technical replicates per experiment). (**J**) FACS analysis of MTG in murine CD4$^+$ T cells and iFoxA1$^+$ T$_{regs}$. $n = 3$ (two mice per experiment). gMFI, geometric mean fluorescence intensity. (**K**) FACS analysis of TMRE of CD4$^+$ T cells and iFoxA1$^+$ T$_{regs}$. CCCP was used as a positive control. $n = 3$ (two mice per experiment). (**L** and **M**) Mitophagy analysis was performed by confocal microscope on CD4$^+$ T cells and iFoxA1$^+$ T$_{regs}$ upon staining with MTG (mitochondria), LTR (lysosomes), and Hoechst (nuclei). (L) The quantification of colocalized mitochondria-lysosome particles (white arrows)/cells/30 min ($n \geq 40$). CCCP, positive control to induce mitophagy. (**N**) LC3B-II FACS (top) and WB (bottom) analysis in CD4$^+$ T cells and iFoxA1$^+$ T$_{regs}$ from WT mice with or without bafilomycin (Baf) (50 nM for 24 hours). LC3B-II turnover (% LC3B), calculated as the difference between Baf and untreated samples, representing LC3B-II accumulating upon lysosome inhibition. Histograms represent means ± SEM. Unpaired multiple *t* tests (H and I); unpaired *t* test (J); one-way analysis of variance (ANOVA) with Tukey's multiple comparison test (K to N). ns, not significant; *$P < 0.05$; **$P < 0.01$; ***$P < 0.001$; ****$P < 0.0001$.

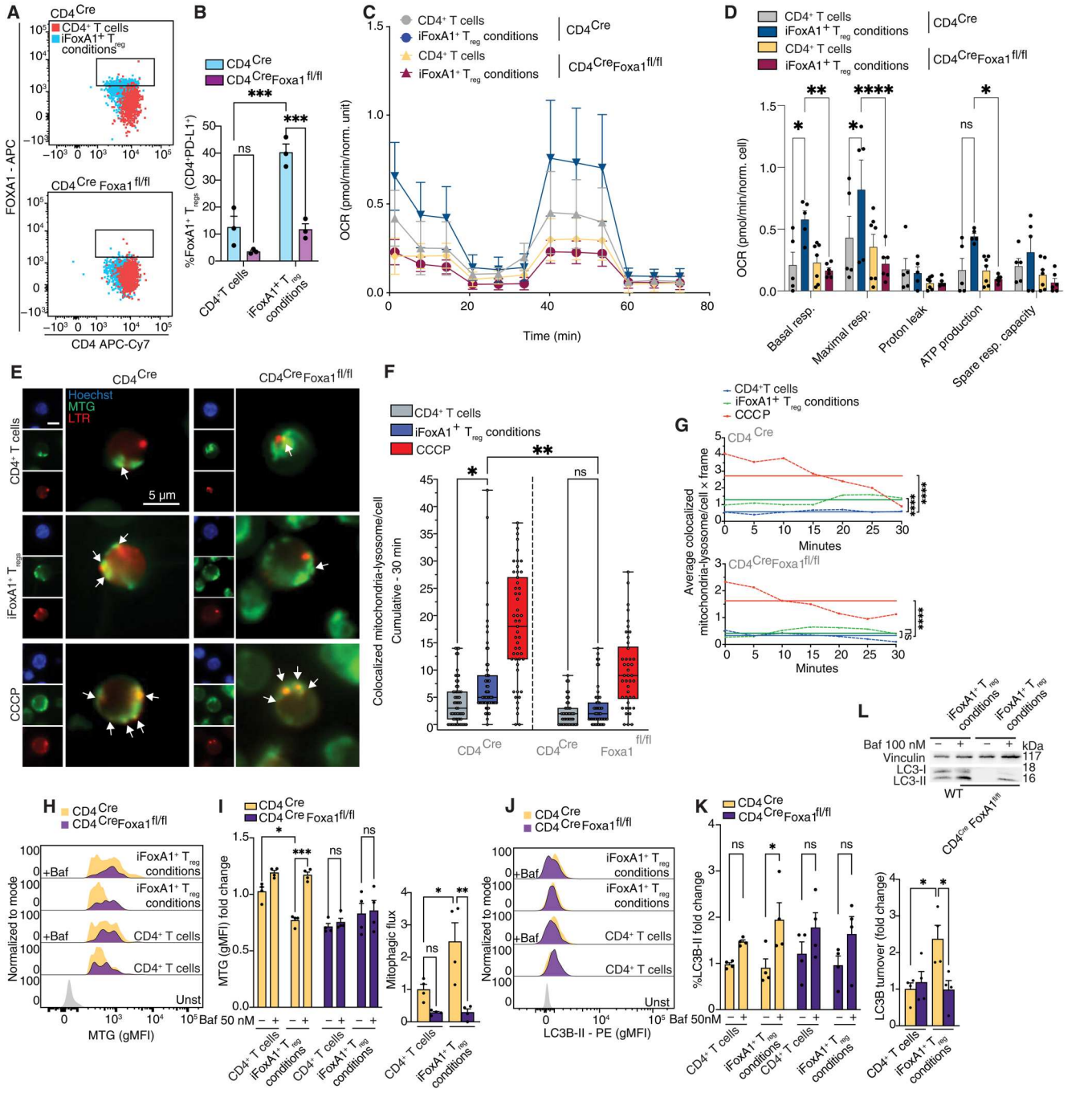

Fig. 2. FoxA1 transcription factor is required for mitochondrial respiration and mitophagy in FoxA1$^+$ T$_{reg}$ differentiation. (**A**) FACS plots of iFoxA1$^+$ T$_{regs}$ in CD4^{Cre} and CD4^{Cre} Foxa1$^{fl/fl}$ mice. (**B**) Quantification of FACS plots is shown in (A) ($n = 3$). (**C** and **D**) Seahorse analysis of OCR on CD4$^+$ T cells and iFoxA1$^+$ T$_{reg}$ conditions from CD4^{Cre} and CD4^{Cre}Foxa1$^{fl/fl}$ mice. $n = 1$ with five to seven technical replicates (10 mice per experiment). (**E**) Representative frames of live-imaging confocal microscopy of CD4$^+$ T cells and iFoxA1$^+$ T$_{regs}$ isolated from CD4^{Cre} and CD4^{Cre}Foxa1$^{fl/fl}$ mice stained with MTG (mitochondria), LTR (lysosomes), and Hoechst (nuclei). White arrows, mitochondria/lysosome colocalization. CCCP, mitophagy inducer. (**F**) Colocalized mitochondria-lysosome particles/cells/30 min ($n \geq 40$). Center line, median; box limits, 25th and 75th percentiles; whiskers, minimum and maximum. (**G**) Average colocalized mitochondria-lysosome/cells ($n \geq 40$) for each time point calculated from (E). (**H** and **I**) FACS analysis of mitochondrial mass of CD4$^+$ T cells and iFoxA1$^+$ T$_{regs}$ isolated from CD4^{Cre} and CD4^{Cre} Foxa1$^{fl/fl}$ mice stained with MTG in the presence or not of Baf (50 nM for 24 hours). Data are shown as representative plots (I) and histograms (J) of $n = 3$ independent experiments. Mitophagy flux calculated as the difference in mitochondrial mass between Baf-treated and untreated samples, expressed as fold change relative to CD4$^+$ T cells. (**J** to **L**) FACS analysis of LC3B-II in CD4$^+$ T cells and iFoxA1$^+$ T$_{regs}$ isolated from CD4^{Cre} and CD4^{Cre} Foxa1$^{fl/fl}$ mice in the presence or not of Baf (50 nM for 24 hours). LC3B-II turnover (% LC3B-II, difference between Baf-treated and untreated samples) in (K) is expressed as fold change with respect to CD4$^+$ T cells. Immunoblot of LC3B in (L). Histograms represent means ± SEM. Two-way ANOVA with Tukey's multiple comparison test (B and G); means ± SD, two-way ANOVA with Tukey's multiple comparison test (C and D). Means ± SD, one-way ANOVA with Šidák's multiple comparison test (F). Means ± SEM, one-way ANOVA Tukey's multiple comparison test (I to K). *$P < 0.05$; **$P < 0.01$; ***$P < 0.001$; ****$P < 0.0001$.

our earlier findings, we observed increased mitochondrial respiration in iFoxA1$^+$ T$_{regs}$ differentiated from WT mice (fig. S1, J and K). This effect was not evident in iFoxA1$^+$ T$_{regs}$ from *Ifnar1*$^{-/-}$ mice, providing strong evidence for the pivotal role of IFNβ-IFNAR1-FoxA1 signaling in the regulation of mitochondrial metabolism. No differences were observed in basal mitochondrial reactive oxygen species production in either WT or *Ifnar1*$^{-/-}$ T cells (fig. S1L).

Since mitochondrial turnover (i.e., mitophagy) controls the health status of cell mitochondrial pool, we performed live imaging under iFoxA1$^+$ T$_{reg}$ conditions from CD4^{Cre} and CD4^{Cre}Foxa1$^{fl/fl}$. Consistent with our previous results, iFoxA1$^+$ T$_{regs}$ from CD4^{Cre} mice showed a significant increased mitophagy flux (Fig. 2, E to G). Conversely, we did not observe the same trend in cells with attempt to generate iFoxA1$^+$ T$_{regs}$ from CD4^{Cre}Foxa1$^{fl/fl}$ mice (Fig. 2, E to G), indicating that mitophagy induction requires FoxA1 transcriptional activity in iFoxA1$^+$ T$_{regs}$. We further analyzed mitochondrial mass changes by staining iFoxA1$^+$ T$_{regs}$ with MTG and detecting the accumulation of lysosome-targeted mitochondria by blocking their degradation with Baf (*39*). In line with data shown in Fig. 1J, we observed a significant reduction of mitochondrial mass in CD4^{Cre}-derived cells under iFoxA1$^+$ T$_{reg}$ conditions (Fig. 2, H and I), which was also recovered with Baf treatment, indicating the accumulation of mitochondria in lysosomes. Noticeably, we did not find any significant difference under iFoxA1$^+$ T$_{reg}$ conditions derived from CD4^{Cre}Foxa1$^{fl/fl}$ mice, which showed a reduced mitophagy rate when compared to their control CD4^{Cre} (Fig. 2, J to L).

Similar result was achieved by measuring LC3B-II turnover. iFoxA1$^+$ T$_{regs}$ isolated from CD4^{Cre} mice showed higher LC3B-II turnover with respect to iFoxA1$^+$ T$_{regs}$ isolated from CD4^{Cre}Foxa1$^{fl/fl}$ mice by FACS and WB analysis (Fig. 2, J to L). Together, these results demonstrate that FoxA1 transcription factor is essential for mitochondrial respiration and mitophagy during FoxA1$^+$ T$_{reg}$ differentiation.

FoxA1 induces PRKAG2 transcription during iFoxA1$^+$ T$_{reg}$ differentiation

To investigate the specific mechanism of FoxA1$^+$ T$_{reg}$ metabolic program induced by IFNβ, we compared the gene profile of human iFoxA1$^+$ T$_{regs}$ with TGFβ-induced FoxP3$^+$ T$_{regs}$, used as a control T$_{reg}$ population (fig. S2A). We selected differentially expressed (DE) genes whose relative expression changed significantly [log fold change (logFC) > |0.25|], revealing a total of 59,368 transcripts that were differentially expressed between iFoxA1$^+$ T$_{regs}$ and iFoxP3$^+$ T$_{regs}$, reflecting that iFoxA1$^+$ T$_{regs}$ and iFoxP3$^+$ T$_{regs}$ are two distinct populations on a fundamental molecular basis (Fig. 3A) (*10*). Key mediators of type I IFN responses (*IFI6*, *IFIT2*, *MX1*, and *MX2*) were identified among the nine mostly up-regulated genes; the remaining are mainly related to cell metabolism: (i) *OMA1* is a metalloendopeptidase localized in the inner membrane of mitochondria, controlling mitochondria quality control system and energy metabolism (*40*); (ii) *COX19* is the cytochrome c oxidase assembly factor required for redox signal to regulate cellular copper homeostasis (*41*); *MT-ND4* and *MT-ND5* are the subunits of the mitochondrial membrane respiratory chain NADH dehydrogenase (complex I), which catalyzes the electron transfer from NADH through the respiratory chain (*42*); Protein Kinase AMP-Activated Non-Catalytic Subunit Gamma 2 (*PRKAG2*) is the γ subunit of AMPK, a master regulator of metabolism (Fig. 3A) (*43*). Collectively, these data suggest that IFNβ signaling has a crucial impact on mitochondrial metabolism during FoxA1$^+$ T$_{reg}$ differentiation.

To address the specific impact of IFNβ on mitochondrial metabolism, we compared hIFNβ-induced iFoxA1$^+$ T$_{regs}$ with classical natural and induced FoxP3$^+$ T$_{reg}$ subsets [activated T$_{regs}$ (aT$_{regs}$), effector T$_{regs}$ (eT$_{regs}$), induced T$_{regs}$ (iT$_{regs}$), and resting T$_{regs}$ (rT$_{regs}$)] used as control groups of T$_{regs}$ (Fig. 3, B and C, and fig. S2A). We aimed to identify the shared genes that IFNβ signal is distinctly regulating in all subsets of FoxP3$^+$ T$_{regs}$ regardless of their own subset specific differences. The transcriptomic profile of selected DE genes based on a logFC > |0.25| showed 11 shared genes that were up-regulated upon IFNβ treatment in all T$_{reg}$ subsets (Fig. 3B). The expression of the selected 11 genes was also represented in a heatmap comparing untreated T$_{reg}$ subsets versus IFNβ-treated T$_{reg}$ subsets (Fig. 3C). Notably, *PRKAG2* was up-regulated in all IFNβ-treated T$_{reg}$ subsets, especially in iFoxA1$^+$ T$_{regs}$, indicating that IFNβ is capable of inducing plasticity in all FoxP3$^+$ T$_{reg}$ subsets and that *PRKAG2* is a potential target of IFNβ signaling. As a validation to RNA-seq data, we found that PRKAG2 protein expression was significantly up-regulated in iFoxA1$^+$ T$_{regs}$ in comparison with iFoxP3$^+$ T$_{regs}$ differentiated from human donors (Fig. 3D and fig. S2B). We also confirmed this finding in cells derived from CD4^{Cre} mice but not in the IFNβ-treated CD4$^+$ T cells derived from CD4^{Cre}Foxa1$^{fl/fl}$ mice, where we found that FoxA1 loss was correlated with a low PRKAG2 expression (Fig. 3E and fig. S1I).

As AMPK activation and phosphorylation rely on the regulatory function of PRKAG2, we examined phosphorylated-AMPK (pAMPK) levels in IFNβ-treated CD4$^+$ T cells isolated from CD4^{Cre}Foxa1$^{fl/fl}$ mice. Notably, we were unable to detect any increase of pAMPK levels in these cells compared to iFoxA1$^+$ T$_{reg}$ conditions from WT mice (fig. S2C). These results underscore the critical role of the FoxA1-PRKAG2 axis in facilitating AMPK phosphorylation during iFoxA1$^+$ T$_{reg}$ differentiation.

We then investigated the involvement of FoxA1 in the regulation of *PRKAG2* gene. To screen for potential FoxA1 targets, we performed chromatin immunoprecipitation sequencing (ChIP-seq) on human iFoxA1$^+$ T$_{regs}$ and human iFoxP3$^+$ T$_{regs}$, followed by immunoprecipitation of genomic DNA fragments with an anti-FOXA1 and anti-FOXP3 antibody, respectively. As hypothesized, FoxA1 binds to *PRKAG2* promoter to a higher extent under IFNβ treatment than in the controls (Fig. 3F), whereas we found few bindings with FOXP3 (fig. S2D). To confirm that FoxA1 regulates the expression of the *PRKAG2* gene, we used CD4^{Cre}Foxa1$^{fl/fl}$ mice and evaluated its expression by qPCR analysis. As shown in Fig. 3G, lack of *Foxa1* led to a remarkable deficiency of *PRKAG2* gene expression. *PRKAG2* expression was not correlated with iFoxP3$^+$ T$_{regs}$ (Fig. 3G). In addition, by analyzing the promoter of *PRKAG1* isoform, we did not find binding regions neither for FoxA1 nor for FoxP3 (fig. S2, E and F). qPCR analysis of *PRKAG1* confirmed that this gene expression is not induced by FoxA1 or FoxP3 (fig. S2G). Last, we performed the isoform usage analysis that denotes the set of relative abundances (proportions of total gene expression) of all isoforms of a gene. As shown in Fig. 3H, we identified ENST00000476632.2 (hereby referred to as PRKAG2.2) as the specific γ2 transcript isoform induced under iFoxA1$^+$ T$_{reg}$ conditions. Overall, these data demonstrate that FoxA1 transcription factor stimulates PRKAG2 transcription—

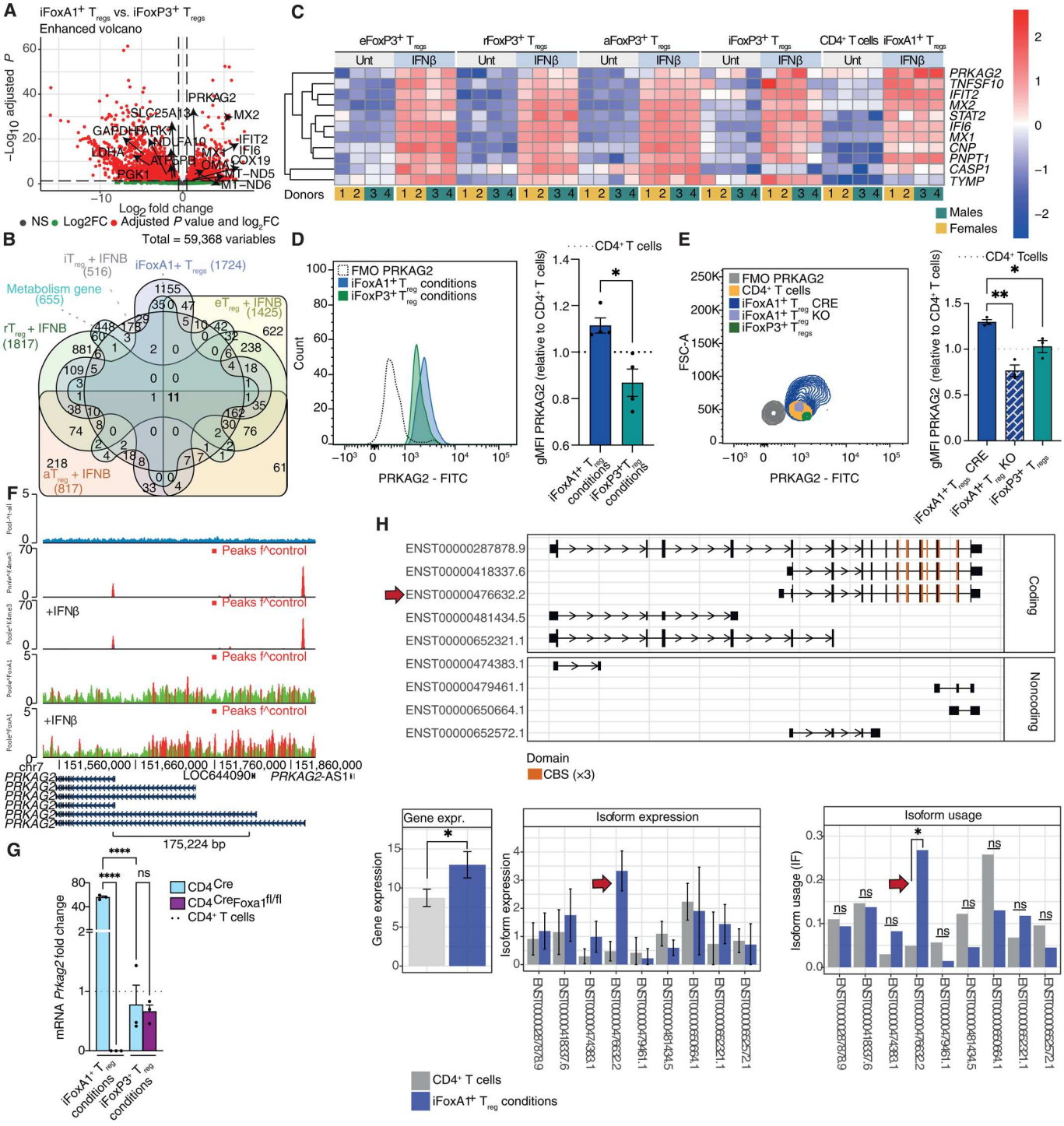

Fig. 3. PRKAG2 is the target of FoxA1 transcription factor during iFoxA1$^+$ T$_{reg}$ differentiation. (**A**) Volcano plot showing DE genes between human iFoxA1$^+$ T$_{regs}$ and iFoxP3$^+$ T$_{regs}$; all DE genes were selected based on a $\log_2$ fold change ($\log_2$FC) > |0.25| and $P < 0.05$. (**B**) Venn diagram of DE genes significantly modulated by IFNβ treatment in FoxP3$^+$ T$_{reg}$ subsets; eFoxP3$^+$ T$_{regs}$, effector FoxP3$^+$ T$_{regs}$; rFoxP3$^+$ T$_{regs}$, resting FoxP3$^+$ T$_{regs}$; aFoxP3$^+$ T$_{regs}$, activated FoxP3$^+$ T$_{regs}$; iFoxP3$^+$ T$_{regs}$, induced FoxP3$^+$ T$_{regs}$. (**C**) Heatmap showing the top 11 DE genes in FoxP3$^+$ T$_{reg}$ subsets described in (B) upon IFNβ treatment; all DE genes were selected on the basis of a $\log_2$FC > |0.25| and $P < 0.05$. (**D**) FACS analysis of PRKAG2 gMFI expression under iFoxA1$^+$ T$_{reg}$ and iFoxP3$^+$ T$_{reg}$ conditions obtained from human donors ($n = 3$ donors). (**E**) gMFI of PRKAG2 under iFoxA1$^+$ and iFoxP3$^+$ T$_{reg}$ conditions obtained from CD4^{Cre} and CD4^{Cre}Foxa1$^{fl/fl}$ mice ($n = 3$). KO, knockout. FSC, FACS forward scatter. (**F**) Genomic tracks display ChIP-seq data in human cells. Data shown describe enrichment profiles for FOXA1 (green), with peaks presenting binding sites to *PRKAG2* promoter (red). (**G**) Reverse transcription qPCR of *Prkag2*, in murine iFoxA1$^+$ T$_{regs}$ and iFoxP3$^+$ T$_{regs}$ isolated from CD4^{Cre} and CD4^{Cre} Foxa1$^{fl/fl}$ mice ($n = 3$). One-way ANOVA with Tukey's multiple comparison test. CBS, cystathionine-beta-synthase. (**H**) Isoform usage analysis of *PRKAG2* transcript variants. Histograms show mean ± SEM, unpaired *t* test (D and E) and one-way ANOVA with Tukey's multiple comparison test (G). *$P < 0.05$; **$P < 0.01$; ****$P < 0.0001$.

preferentially, the transcript variant PRKAG2.2—in an IFNβ-dependent manner exclusively in FoxA1$^+$ T_{regs}.

PRKAG2.2 selectively drives iFoxA1$^+$ T_{reg} differentiation

We then investigated whether PRKAG2.2 was involved in iFoxA1$^+$ T_{reg} differentiation. Since AMPK is an important general driver of T cell activation and cytokine production and it controls T cell metabolic plasticity (*44*), we started our inquiry by inhibiting AMPK activity during human iFoxA1$^+$ T_{reg} and iFoxP3$^+$ T_{reg} differentiation using compound C (also known as dorsomorphin), a widely used AMPK inhibitor (Fig. 4, A to C) (*45*). Our results show that AMPK is also crucial for FoxA1$^+$ T_{reg} differentiation in the same manner as FoxP3$^+$ T_{reg} differentiation (*46*). To establish the selective role of the PRKAG2.2 variant in the differentiation of iFoxA1$^+$ T_{regs} and iFoxP3$^+$ T_{regs}, we designed a small interfering RNA (siRNA) against this transcript variant and analyzed cell differentiation after 48-hour silencing. Our results show that a successful PRKAG2.2 silencing inhibited the differentiation of iFoxA1$^+$ T_{regs} selectively, but it had no impact on iFoxP3$^+$ T_{regs} that still showed capacity to differentiate (Fig. 4, D to H). These data clearly established that the PRKAG2.2 variant plays an exclusive role in iFoxA1$^+$ T_{reg} differentiation but not in iFoxP3$^+$ T_{regs}.

To assess the impact of PRKAG2.2 during proliferation, stability, and maintenance of FoxA1$^+$ T_{regs}, we isolated CD4$^+$ T cells from WT mice and differentiated FoxA1$^+$ T_{regs} in the presence or absence of siPRKAG2.2 as described in fig. S3 (A and D). Our findings reveal that the silencing of PRKAG2.2 had no effects on proliferation or stability of FoxA1$^+$ T_{regs} during differentiation (fig. S3, B and E). It is worth noting that, as we previously reported (*10*), upon FoxA1$^+$ T_{reg} differentiation, the proliferation rate of cells decreases

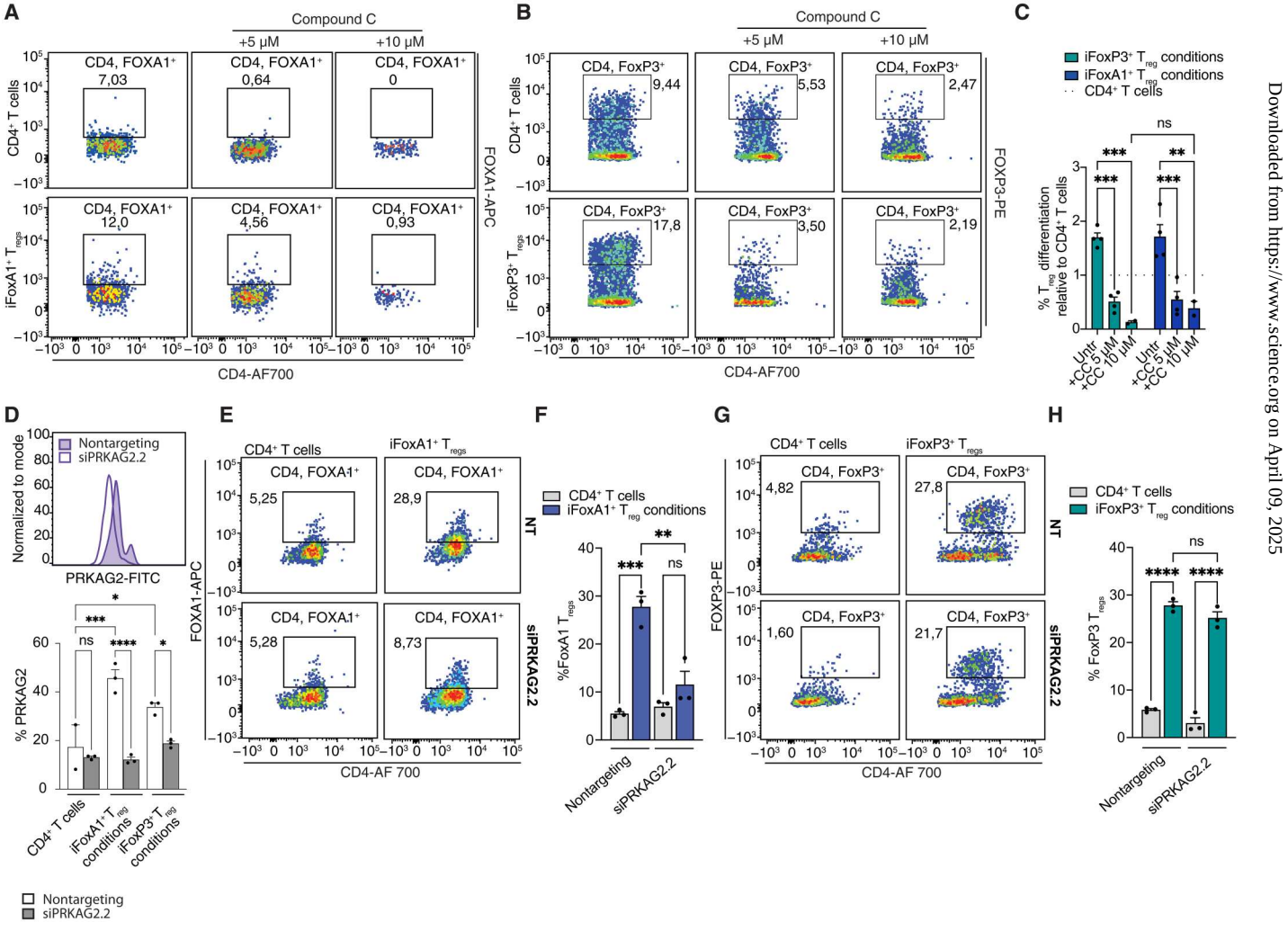

Fig. 4. PRKAG2.2 plays distinctive role in FoxA1$^+$ T_{reg} differentiation. Human CD4$^+$ T cells were treated for 48 hours either with hIFNβ or with hTGFβ + interleukin-2 (IL-2) to induce FoxA1$^+$ T_{regs} and FoxP3$^+$ T_{regs}, respectively. (**A** and **B**) FACS plots of iFoxA1$^+$ (A) and iFoxP3$^+$ (B) T_{reg} differentiation treated or not with 5 mM/10 mM of compound C for the last 24 hours of culture. (**C**) Quantification of FACS plot in (A) and (B), expressed as %T_{reg} differentiation relative to CD4$^+$ T cells. (**D**) FACS histogram showing PRKAG2.2 silencing (siPRKAG2.2) in human CD4$^+$ T cells, iFoxA1$^+$ T_{regs} and iFoxP3$^+$ T_{regs} compared to nontargeting control. (**E** and **G**) FACS analysis of iFoxA1$^+$ T_{reg} (E) and iFoxP3$^+$ T_{reg} (G) differentiation upon siPRKAG2.2 compared with nontargeting (NT) siRNA control. Representative FACS plots and histograms show one representative donor (performed in three technical replicates) of three independent experiments. (**F** and **H**) Histograms showing the quantification of (E) and (G). Histograms represent means ± SEM analyzed by one-way ANOVA with Tukey's multiple comparison test (C, D, F, and H). *P < 0.05; **P < 0.01; ***P < 0.001; ****P < 0.0001.

when compared to $CD4^+$ T cells. In addition, silencing PRKAG2.2 before or after $FoxA1^+$ T_{reg} differentiation did not show any significant differences in cell death based on annexin V expression analysis (fig. S3, C and F). Together, our data solidly established that the PRKAG2.2 variant is detrimental for $iFoxA1^+$ T_{reg} differentiation, but postdifferentiation is not affecting cell proliferation/apoptosis.

PRKAG2.2 sustains $iFoxA1^+$ T_{reg} mitochondrial respiration and turnover

We showed that PRKAG2.2 affected $iFoxA1^+$ T_{reg} but not $iFoxP3^+$ T_{reg} differentiation. Because of PRKAG2.2 role in regulating AMPK and thus mitochondrial metabolism, we analyzed the bioenergetic profile of $iFoxA1^+$ T_{regs} and $iFoxP3^+$ T_{regs} isolated from human healthy donors upon silencing PRKAG2.2 for 48 hours. Mitochondrial respiration was significantly repressed by siPRKAG2.2 transfection under $iFoxA1^+$ T_{reg} conditions, but it was not changed in $iFoxP3^+$ T_{regs} (Fig. 5, A and B).

As AMPK is also involved in mitophagy induction (*47*), we next investigated whether mitophagy was driven by PRKAG2.2 in $iFoxA1^+$ T_{regs}. Live imaging microscopy analyses showed that mitophagy was significantly reduced in PRKAG2.2-silenced $iFoxA1^+$ T_{regs} while we detected no differences in $iFoxP3^+$ T_{regs} (Fig. 5, C to F). Moreover, analyses of mitophagy flux and LC3B-II turnover upon PRKAG2.2 silencing confirmed that mitophagy depends on this transcript variant in $iFoxA1^+$ T_{regs} but not in $iFoxP3^+$ T_{regs} (Fig. 5, G to L). In addition, in this case, we did not detect any difference in p62 expression (fig. S3G), indicating that p62 does not play a central role in mitophagy during T_{reg} differentiation and PRKAG2.2 regulation. Overall, our results indicate that PRKAG2.2 selectively sustains $iFoxA1^+$ T_{reg} mitochondrial respiration and turnover during differentiation.

FoxA1-PRKAG2.2 axis activates AMPK signaling and BNIP3-mediated mitophagy

PRKAG2, the regulatory γ2 subunit of AMPK, plays a crucial role in cells that require energy and are involved in energy-producing or energy-consuming processes, allowing them to adapt and respond to changes in cellular energy status (Fig. 6A) (*21*). As PRKAG2 it is more responsive to changes in AMP and ADP compared to the γ1 subunit, cells expressing high PRKAG2 can quickly adjust their metabolic rate based on their needs (*23*). To substantiate the activation of AMPK during $iFoxA1^+$ T_{reg} differentiation, we quantified energetic cofactors ADP/ATP and NAD^+/NADH, the important electron carriers, shuttling electron from glycolysis and the citric acid to the electron transport chain. We observed an increase in ADP/ATP ratio in mouse $iFoxA1^+$ T_{regs} but not in $iFoxP3^+$ T_{regs} (Fig. 6B), and this was pointing toward an energetic status favorable to AMPK activation. However, we did not find any differences in NAD^+/NADH ratio neither in $iFoxA1^+$ T_{regs} nor in $iFoxP3^+$ T_{regs} (fig. S3H).

Next, we investigated whether PRKAG2.2 induction stimulated by IFNβ correlated with an increase in AMPK activity. WB and FACS analysis showed that AMPK phosphorylation—on an activation site—and the phosphorylation of one of AMPK main targets, Unc-51-like kinase 1 (ULK1) (*48*, *49*), were increased in $iFoxA1^+$ T_{regs} while not affected in $iFoxP3^+$ T_{regs} (Fig. 6, C to E, and fig. S4, A and B). PRKAG2.2 silencing abolished these activator post-translational modifications (Fig. 6, C to E), demonstrating a notable regulation of AMPK pathway driven by PRKAG2.2 variant exclusively under $iFoxA1^+$ T_{reg} condition. Differently, PRKAG2.2 depletion did not exert any relevant effect on the phosphorylation states of Raptor and Beclin (fig. S4, C to G), two other targets of AMPK implicated in the inhibition of mammalian target of rapamycin complex 1 (mTORC1) signaling and regulation of autophagy, respectively (*50*, *51*). AMPK-mediated phosphorylation of Ser^{555} in ULK1 kinase stimulates several mitophagy adaptors and plays an important role in initiating autophagosome membrane formation around damaged/exhausted mitochondria (*52*).

Mitophagy can be initiated through both PINK1 (PTEN-induced putative kinase 1)–PRKN (Parkin RBR E3 ubiquitin protein ligase)–dependent and –independent pathways (*53*). To investigate their plausible involvement, WB analysis of p62, PINK1, and PRKN expression was performed. We did not find differences neither in PRKAG2.2-silenced $iFoxA1^+$ T_{regs} nor in $iFoxP3^+$ T_{regs} (fig. S4, H to P), indicating that PINK1-PRKN–dependent pathway is not driving mitophagy during $iFoxA1^+$ T_{reg} differentiation. We did not also find differences in optic atrophy-1 (OPA1) and mitofusin-2 (fig. S4, K to P) that are involved in mitochondrial cristae remodeling and network dynamics (*54*–*56*). We therefore analyzed whether BH3 domain–containing BCL2 family member (BNIP3), as a marker of PINK1-PRKN–independent mitophagy pathway, has a role in the induction of mitophagy during $iFoxA1^+$ T_{reg} differentiation. This approach was motivated since BNIP3 is shown to be stabilized by activated ULK1 to promote natural killer T cells generation via mitophagy induction (*57*). Our data here show that $iFoxA1^+$ T_{regs} increased BNIP3 levels, whereas we did not observe any changes in $iFoxP3^+$ T_{regs} (Fig. 6, F and G). PRKAG2.2 silencing significantly reduces BNIP3 accumulation upon Baf treatment in $iFoxA1^+$ T_{regs} (Fig. 6, F and G). BNIP3-mediated mitophagy relies on an active autophagic flux and the interaction with LC3 (*58*, *59*). Our results show that $iFoxA1^+$ T_{regs} have a significant LC3 turnover that can be blocked by silencing PRKAG2.2, while in $iFoxP3^+$ T_{regs}, autophagy flux is not affected upon PRKAG2.2 silencing (Fig. 6, F to H).

To further confirm the involvement of ULK1-BNIP3 pathway in $iFoxA1^+$ T_{regs}, we silenced BNIP3 during T_{reg} differentiation. BNIP3 silencing had a broad effect since it reduced the generation of both $iFoxA1^+$ T_{regs} and $iFoxP3^+$ T_{regs} (fig. S5, A to G), and it caused a decrease in mitochondrial respiration in all studied T cell populations, $iFoxA1^+$ T_{regs}, $iFoxP3^+$ T_{regs}, and control $CD4^+$ T cells (Fig. 6, I and J). The loss of BNIP3 modulated mitophagy by reducing the number of mitochondria [detected with Translocase of the outer mitochondrial membrane complex subunit 20 (anti-TOM20) antibody] within autophagosomes ($LC3^+$ puncta), in $iFoxA1^+$ T_{reg} but not in $iFoxP3^+$ T_{reg} (Fig. 6, K and L).

This result was also confirmed by analyzing MTG (Fig. 6, M to O) where mitochondrial mass is only accumulated in $iFoxA1^+$ T_{regs} following Baf treatment; this accumulation was not observed after BNIP3 silencing, confirming its involvement in mitophagy during $iFoxA1^+$ T_{reg} differentiation. Differently, in $iFoxP3^+$ T_{regs}, there was no accumulation of MTG upon Baf treatment (Fig. 6, M and N), indicating that BNIP3 silencing had no effect. On the other hand, LC3 expression was reduced under both $iFoxA1^+$ T_{reg} and $iFoxP3^+$ T_{reg} conditions after BNIP3 silencing (fig. S5, H and I). This suggests that BNIP3 is important in both cell types exerting different functions; likely by targeted mitophagy regulation only in $iFoxA1^+$ T_{regs}, while autophagy is regulated in both T_{reg} populations.

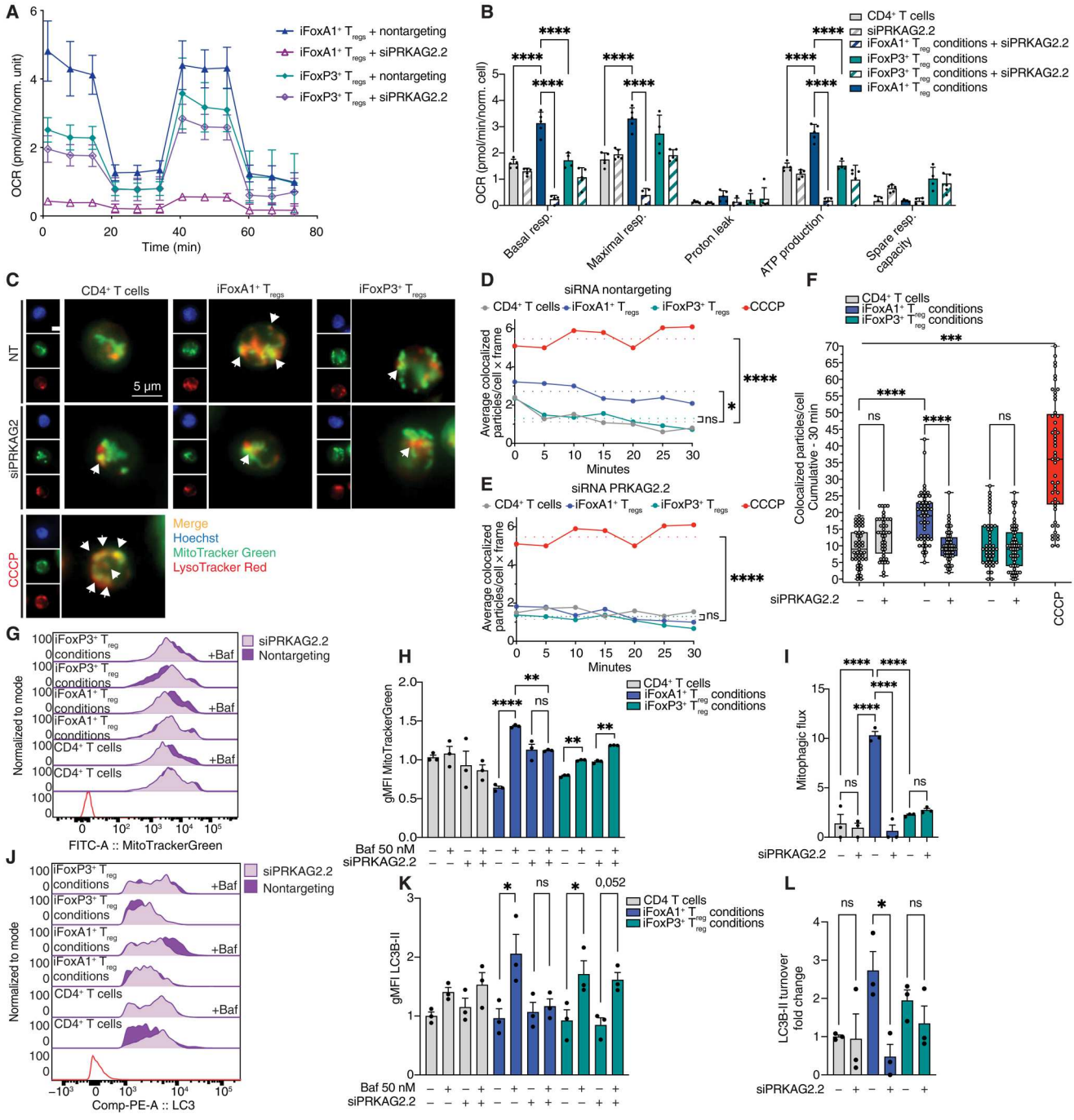

Fig. 5. PRKAG2.2 is specific for FoxA1$^+$ T_{reg} metabolism and mitochondria homeostasis. (**A** and **B**) Seahorse analysis of OCR performed on CD4$^+$ T cells and iFoxA1$^+$ T_{regs} obtained from human donors upon silencing of PRKAG2.2 or transfected with a nontargeting sequence. The graph shows one representative out of three independent experiments performed on three donors. (**C**) Representative frames of live-imaging confocal microscopy of CD4$^+$ T cells and iFoxA1$^+$ T_{regs} obtained from one human donor upon staining with MTG (mitochondria), LTR (lysosomes), and Hoechst (nuclei). White arrows highlight mitochondria/lysosome colocalization. CCCP, mitophagy inducer. (**D** and **E**) Average number of colocalized mitochondria-lysosome/cells ($n \geq 40$) for each time point and experimental condition calculated from (C). (**F**) Box plots showing the cumulative quantification of colocalized mitochondria-lysosome/cells/30 min ($n \geq 40$). Center line, median; box limits, 25th and 75th percentiles; whiskers, minimum and maximum. (**G** and **H**) FACS analysis of total mitochondrial mass of CD4$^+$ T cells and iFoxA1$^+$ T_{regs} obtained from human donors upon silencing of PRKAG2.2 or transfected with a nontargeting sequence. Cells were treated or not with Baf (50 nM for 24 hours) and stained with MTG ($n = 3$). (**I**) Mitophagy flux was calculated as the difference in mitochondrial mass between Baf-treated and untreated samples, expressed as fold change relative to human CD4$^+$ T cells. (**J** to **L**) LC3B-II FACS analysis on CD4$^+$ T cells and iFoxA1$^+$ T_{regs} obtained from human donors upon silencing of PRKAG2.2 or transfected with a nontargeting sequence, in the presence or not of Baf (50 nM for 24 hours). LC3B-II turnover (% LC3B-II, difference between Baf and untreated samples) in (L) is expressed as fold change with respect to CD4$^+$ T cells. Histogram represents means ± SEM. Unpaired multiple *t* tests (B), two-way ANOVA with Šidák's multiple comparison test (D and E), one-way ANOVA with Tukey's multiple comparison test (F, K, and L), and two-way ANOVA with Tukey's multiple comparison test (H and I). *$P < 0.05$; **$P < 0.01$; ***$P < 0.001$; ****$P < 0.0001$.

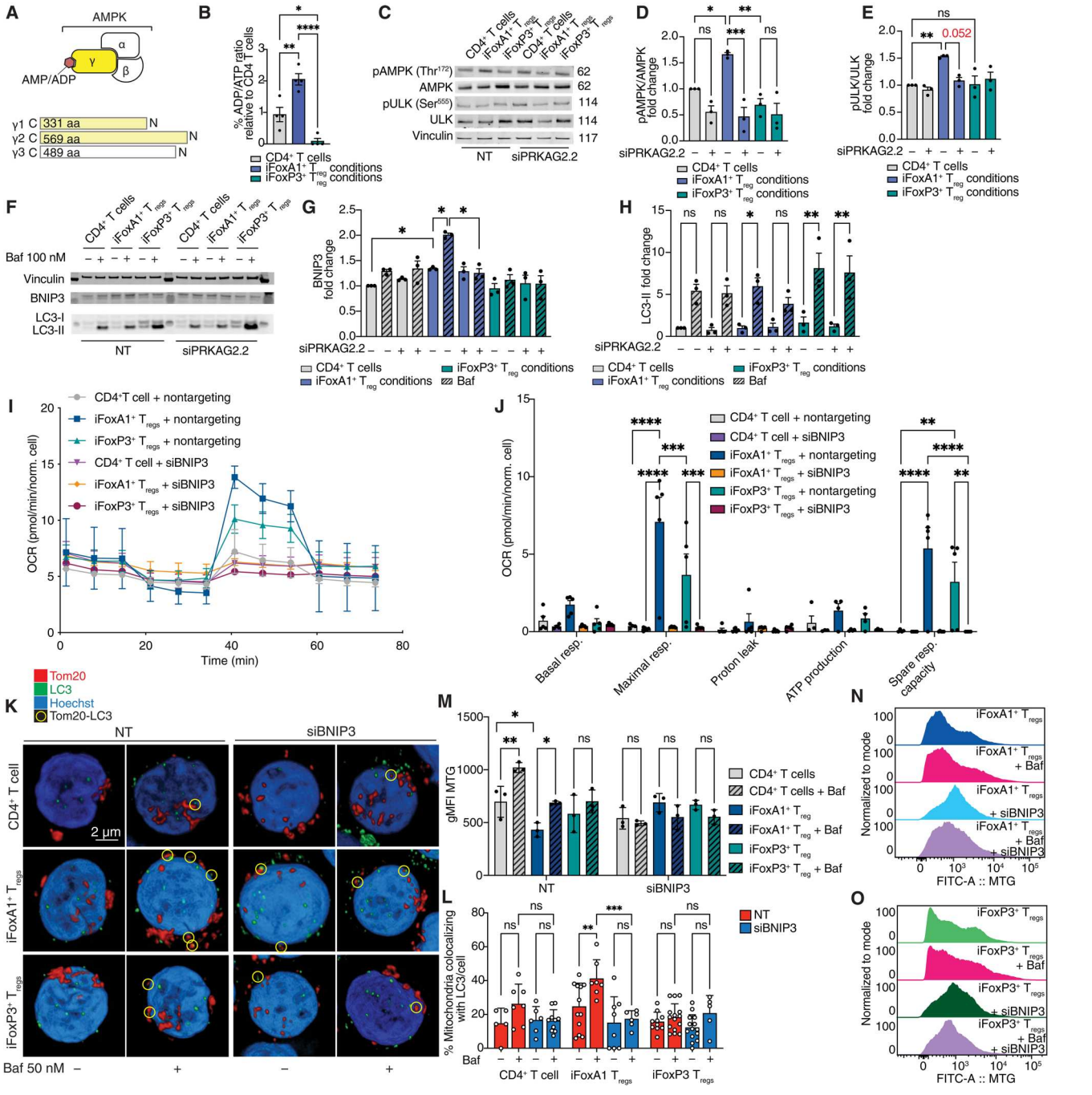

Fig. 6. FoxA1-PRKAG2.2 axis controls mitochondria homeostasis through ULK-BNIP3 regulation in iFoxA1$^+$ T$_{regs}$. (**A**) Schematic representation of AMPK structure. Graphic representation of *PRKAG2* isoforms length (bottom). aa, amino acid. (**B**) ADP/ATP relative ratio calculated with bioluminescent assay in murine CD4$^+$ T cells, iFoxA1$^+$ T$_{regs}$, and iFoxP3$^+$ T$_{regs}$ (n = 3). (**C** to **E**) Immunoblots of AMPK, ULK, and their phosphorylated forms (phospho-AMPKα Thr^{172} and phospho-ULK Ser^{555}) on CD4$^+$ T cells, iFoxA1$^+$ T$_{regs}$, and iFoxP3$^+$ T$_{regs}$ isolated from human donors upon silencing of PRKAG2.2 or transfected with a nontargeting sequence (NT). Vinculin was used as a loading control. pAMPK/AMPK and pULK/ULK ratios are shown in (D) and (E) (n = 3 donors). (**F** to **H**) Immunoblots of LC3B and BNIP3 alongside the densitometric analysis of bands (G and H) on siPRKAG2.2- or NT-transfected CD4$^+$ T cells and iFoxA1$^+$ and iFoxP3$^+$ T$_{regs}$ isolated from human donors in the presence or not of Baf (50 nM for 24 hours). Vinculin was used as a loading control (n = 3 donors). (**I** and **J**) Seahorse analysis of OCR on CD4$^+$ T cells and iFoxA1$^+$ T$_{regs}$ obtained from human donors upon silencing of BNIP3 or NT (one representative donor with five technical replicates). (**K**) Representative two-dimensional (2D) projections of super-resolution confocal images of human CD4$^+$ T cells, with or without Baf (50 nM for 24 hours). Mitochondria were stained with anti-TOMM20 (red) and autophagosome with anti-LC3B antibodies (green) and nuclei with Hoechst (blue). Yellow circles represent mitochondria overlapping >10% with autophagosomes. (**L**) Quantification of the percentage of mitochondrial colocalizing with LC3/cell in images represented in (K). (**M** to **O**) FACS analysis of total mitochondrial mass on siPRKAG2.2- or NT-transfected CD4$^+$ T cells, iFoxA1$^+$ T$_{regs}$, and iFoxP3$^+$ T$_{regs}$ from human donors. Cells were treated or not with Baf (50 nM for 24 hours) and stained with MTG. Histogram represents the means ± SEM. One-way ANOVA with Tukey's multiple comparison test (B, D, E, G, H, and M), unpaired multiple t tests (J), and one-way ANOVA with Šidák's multiple comparison test (L). *P < 0.05; **P < 0.01; ***P < 0.001; ****P < 0.0001.

The suppressive function of FoxA1$^+$ T_{regs} relies on FoxA1-PRKAG2.2-BNIP3 axis

FoxA1$^+$ T_{regs} have the capability to attenuate neuroinflammation. As documented previously, the suppressive function of FoxA1$^+$ T_{regs} primarily depends on FoxA1 and PD-L1 (*10*). Here, we used an in vitro suppression assay to confirm the suppressive activity of iFoxA1$^+$ T_{regs}. Labeled myelin oligodendrocyte glycoprotein peptide 35 to 55 ($MOG_{35–55}$)–specific autoreactive T cells with cell tracer served as responder cells. Our results demonstrate that iFoxA1$^+$ T_{regs} effectively suppressed the proliferation of $MOG_{35–55}$-specific autoreactive T cells, whereas IFNβ-treated FoxA1-deficient CD4$^+$ T cells failed to exhibit suppressive activity (Fig. 7A and fig. S5, J and M). This result reemphasizes the critical role of FoxA1 in conferring suppressive function of iFoxA1$^+$ T_{regs}.

Next, we investigated the roles of newly identified FoxA1-downstream molecules; PRKAG2.2 and BNIP3 in regulating the suppressive activity of FoxA1$^+$ T_{regs} by silencing PRKAG2.2 or BNIP3 in iFoxA1$^+$ T_{regs} (Fig. 7B and fig. S5, K to M). As expected, iFoxA1$^+$ T_{regs} effectively suppressed the proliferation of $MOG_{35–55}$ -specific autoreactive T cells, whereas the silencing of both PRKAG2.2 and BNIP3 abolished their suppressive capacity (Fig. 7B and fig. S5, K to M) underscoring their crucial role in regulating the suppressive function of iFoxA1$^+$ T_{regs}.

Overall, our results presented here established that the FoxA1-PRKAG2.2 axis stimulates AMPK activation and sustaining mitophagy through the ULK1-BNIP3 pathway, which are central and specific for differentiation and fate determination of iFoxA1$^+$ T_{regs} distinct from iFoxP3$^+$ T_{regs} (Fig. 7C).

DISCUSSION

FoxA1$^+$ T_{regs} express a cell-lineage determining factor, FoxA1 (hepatocyte nuclear factor 3α) (*10*), a transcription factor (*60*) involved in embryonic and hepatocyte development, stem cell differentiation, and cancer epigenetics (*61*–*65*). We have previously shown that IFNβ is the cytokine able to generate iFoxA1$^+$ T_{regs} through the phosphatidylinositol 3-kinase–AKT–FoxA1 axis (*12*). Ablation of *Foxa1* in mature mouse β cells leads to impaired glucose homeostasis and insulin secretion (*66*); however, whether IFNβ affects metabolism to generate FoxA1$^+$ T_{regs} was not yet established. In this study, we describe that IFNβ-FoxA1 axis induces the expression of the transcription variant 2.2 of the AMPK γ2 subunit (PRKAG2.2) promoting the metabolic rewiring and mitochondrial turnover needed for iFoxA1$^+$ T_{reg} differentiation, associated with ULK1-BNIP3 axis.

In support of our findings, type I IFNs were reported to play a role in cellular metabolism by increasing OXPHOS during pDC differentiation (*67*). In our current study, in agreement with our previous reports (*10*, *12*), we have reestablished that the differentiation of iFoxA1$^+$ T_{regs} is guided by FoxA1. In addition, we determined that the induction of FoxA1 leads to a significant enhancement of OXPHOS. On the basis of our findings showing a reduction of mitochondrial mass in FoxA1$^+$ T_{regs} together with high mitochondrial membrane potential and OXPHOS, we speculate that FoxA1$^+$ T_{regs} require an increase in functional mitochondria to maintain efficient oxidative metabolism.

Proliferating T cells require metabolic programs compatible with their functional demands (*68*). In this context, the multisubunit kinase AMPK was found to serve as a checkpoint in regulating T cell function and fate (*44*, *69*). Although FoxA1$^+$ T_{regs} are nonproliferative (*10*) in contrast to initial proliferative status of FoxP3$^+$ T_{regs} (*70*), we found support for the importance of AMPK in differentiation of both T_{reg} populations. In line, our analysis showed that AMPK inhibition by compound C decreases both iFoxA1$^+$ T_{reg} and iFoxP3$^+$ T_{reg} differentiation. However, AMPK studies in immune cells are still under debate, and the role of AMPK subunits in T cells is controversial (*71*). It has been demonstrated that AMPKα1 maintains the immunosuppressive function of FoxP3$^+$ T_{regs} and protects against autoimmune liver disease (*72*), but AMPKα1 up-regulation in tumor-infiltrating FoxP3$^+$ T_{regs} prevents antitumor T cell response and promotes tumor progression (*46*). Our study provides novel evidence that a specific AMPK subunit variant γ2.2 determines the differentiation of the distinct T_{reg} population, namely, FoxA1$^+$ T_{regs} but not classical FoxP3$^+$ T_{regs}. Evidence from literature suggests that AMPK has the capability to regulate and stabilize transcription factors (*73*, *74*). Although we show that FoxA1 in response to IFNβ treatment stimulates PRKAG2.2 transcription and AMPK activation, it cannot be excluded that active AMPK may also serve as an upstream inducer of FoxA1 itself. This intriguing scenario suggests a potential regulatory loop in which AMPK might govern FoxA1-dependent transcription, which, in turn, regulates AMPK activity through PRKAG2.2.

Our data also suggest that iFoxA1$^+$ T_{reg} differentiation highly depends on the capacity of cells to remove damaged mitochondria via mitophagy. There are only few studies about the impact of PRKAG2 on autophagy/mitophagy while not addressing PRKAG2.2 variant. In a *Drosophila* model, PRKAG2 homolog SNF4Aγ, is required for regulation of development and stress-induced autophagy (*75*, *76*). Furthermore, PRKAG2 is targeted by transcription factor EB, a master regulator of lysosome biogenesis and mitophagy, indicating a complex interplay between metabolism and these cellular processes (*77*). Nonetheless, no data were so far available on the role played by PRKAG2 or particularly PRKAG2.2 variant in T cells.

Here, we demonstrate that FoxA1 binds and induces the transcription of PRKAG2.2, and this induces the activation of AMPK pathway, leading to a selective boost in mitochondria respiration, ATP production, and the selective removal—via mitophagy—of exhausted mitochondria exclusively in iFoxA1$^+$ T_{regs}. Among the plethora of proteins regulated by AMPK, we further identified ULK1 phosphoactivation at Ser^{555} during iFoxA1$^+$ T_{reg} differentiation. ULK1 activation is critical for the initiation of autophagosome formation and for the stabilization of BNIP3 (*52*) during mitophagy. BNIP3 serves directly as a mitophagy receptor through the binding to LC3B on autophagosomes (*78*–*80*), thus mediating the recruitment of autophagosomes to dysfunctional mitochondria. Our results support a role for ULK1-BNIP3 axis associated with mitophagy regulation in iFoxA1$^+$ T_{regs}.

When we silenced BNIP3, we observed an impairment in mitophagy exclusively in FoxA1$^+$ T_{regs}, but not in FoxP3$^+$ T_{regs}. However, it is worth noting that BNIP3 silencing affected mitochondrial respiration and LC3 turnover in both cell types. Previous studies have shown that depletion of BNIP3 leads to the accumulation of abnormal mitochondria, a decrease in mitochondrial membrane potential, an increase in reactive oxygen species production, and a reduction in ATP generation, resulting in impaired self-renewal and differentiation in mouse embryonic stem cells (*59*).

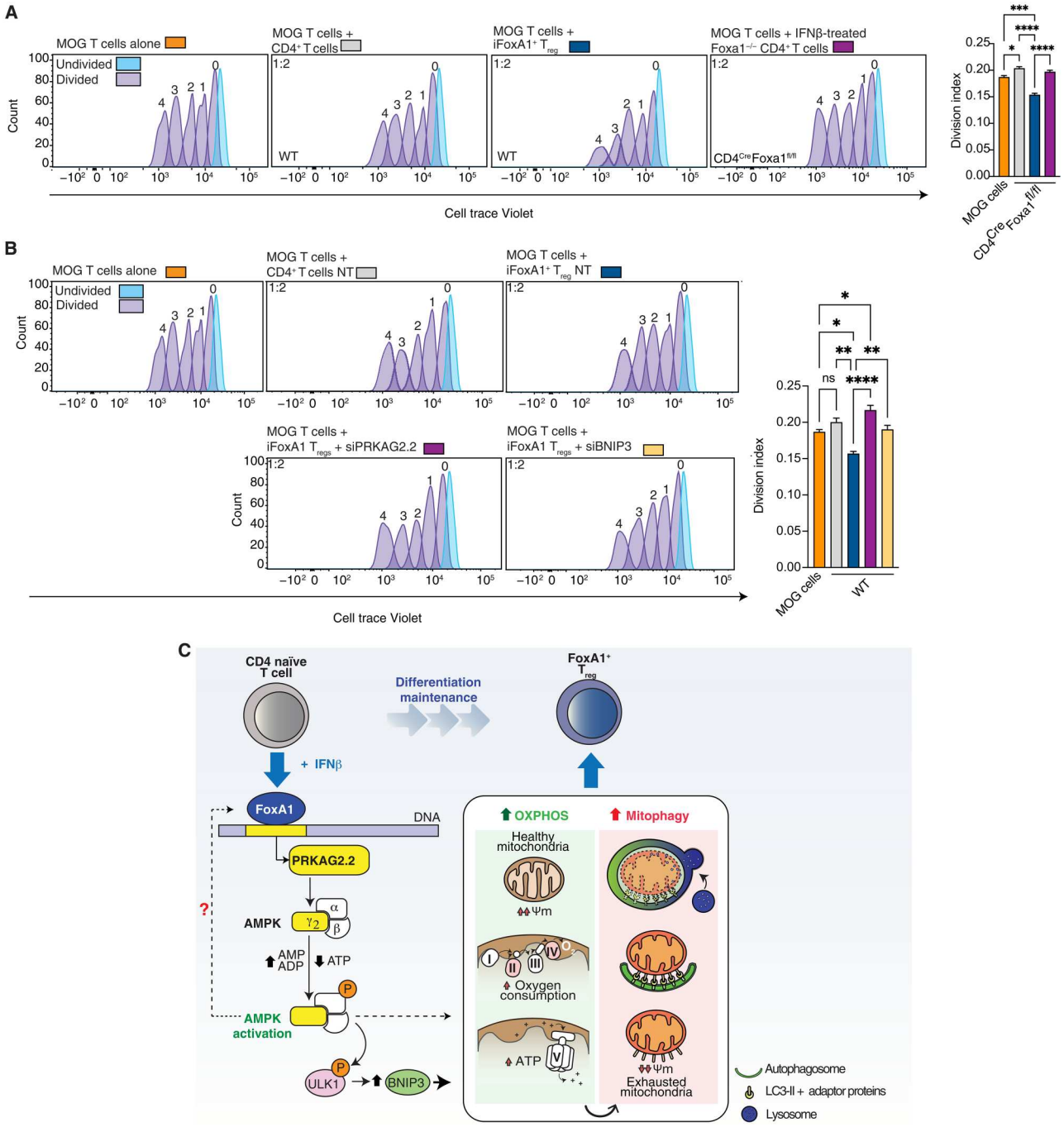

Fig. 7. The suppressive function FoxA1$^+$ T$_{regs}$ relies on FoxA1-PRKAG2.2 axis. (**A**) In vitro suppression assay of iFoxA1$^+$ T$_{regs}$ isolated from WT mice and IFNβ-treated FoxA1-deficient CD4$^+$ T cells isolated from CD4^{Cre} Foxa1$^{fl/fl}$ mice. MOG$_{35–33}$-reactive T cells have been used as responders and labeled with CellTrace violet to quantify their proliferation rate after 48 hours of coculture with iFoxA1$^+$ T$_{regs}$. Data represent one experiment in three technical replicates. (**B**) In vitro suppression assay of iFoxA1$^+$ T$_{regs}$ obtained from CD4$^+$ T cells (WT mice). Where specified, iFoxA1$^+$ T$_{regs}$ have been silenced with siPRKAG2.2 or siBNIP3 for 48 hours. MOG$_{35–55}$-reactive T cells have been used as responder cells, coculture with iFoxA1$^+$ T$_{regs}$ and detected by FACS after 48 hours. The division index is the average number of cell divisions that a cell in the original population has undergone. Data represent one experiment in three technical replicates. Histograms represent means ± SEM. One-way ANOVA with Tukey's multiple comparison tests (A and B). *P < 0.05; **P < 0.01; ***P < 0.001; ****P < 0.0001. (**C**) Schematic representation of the role of IFNβ-FoxA1-PRKAG2.2 axis in iFoxA1$^+$ T$_{reg}$ metabolic rewiring. CD4$^+$ T cells treated with IFNβ differentiate into FoxA1$^+$ T$_{regs}$ by activating FoxA1 transcription factor. FoxA1 binds *PRKAG2* promoter inducing the transcription of the isoform *PRKAG2.2*, a subunit of AMPK thus stimulating its catalytic activity. AMPK activation boosts the activity of healthy mitochondria, characterized by high mitochondrial intermembrane potential (⇑ψ_m), and stimulates mitochondrial OXPHOS, hence oxygen consumption and ATP production. Highly active mitochondria are subjected to deterioration owing to their metabolic activity. IFNβ treatment, by activating AMPK, enhances mitochondrial turnover by recycling exhausted mitochondria via mitophagy, through the phosphorylation of ULK1 and the consequent up-regulation of the mitophagy adapter BNIP3. Consequently, FoxA1$^+$ T$_{reg}$ differentiation induced by IFNβ relies on a pool of healthy metabolically active mitochondria, integrity of which is preserved by a potentiated mitophagy flux.

Our findings indicate that mitophagy is selectively involved in the differentiation of FoxA1$^+$ T_{reg} but does not play a crucial role in FoxP3$^+$ T_{reg} differentiation. This distinction is likely due to differences in the proliferative capacity of these T_{reg} populations. As a result, when we silenced BNIP3, no noticeable effect on FoxP3$^+$ T_{regs} was detected.

In conclusion, our data presented here establishes strong evidence that FoxA1$^+$ T_{reg} differentiation is driven by FoxA1-mediated AMPK activation via targeting PRKAG2.2, that, on one hand, boosts mitochondrial respiration, and, on the other, promotes mitophagy turnover, via activation of phosphorylated ULK1 and BNIP3 axis. This is not excluding a plausible scenario in which PRKAG2.2-mediated AMPK activation could promote mitochondrial biogenesis, as a mechanism to replace exhausted organelles that are recycled by mitophagy. In support, despite a decrease in mitochondrial mass during iFoxA1$^+$ T_{reg} differentiation, we found a massive increase in the metabolic rate of cells and unchanged levels of mitochondrial DNA. Together, our findings depict a circumstance in which PRKAG2.2 expression is exclusively regulated by IFNβ-FoxA1 axis, which, in turn, maintains a pool of healthy and fully functional mitochondria by regulating mitochondrial metabolic rewiring and controlling the clearance of damaged/exhausted mitochondria. Last, our finding on IFNβ-induced FoxA1-PRKAG2.2-BNIP3 interaction revealed a new level on the regulation of specific anti-inflammatory FoxA1$^+$ T_{reg} differentiation, homeostasis, and suppressive function. This is projecting toward the specific management of cellular metabolic pathways as a novel tool in autoimmune disease therapy.

MATERIALS AND METHODS

Mice

WT mice in a C57BL/6 J and *Ifnar1*$^{-/-}$ were inbred at University of Copenhagen by the Department of Experimental Medicine. CD4^{Cre}-Foxa1$^{fl/fl}$ (*81*) and CD4^{Cre} mice—in a C57BL/6J BomTac background—were backcrossed over 20 generations, and WT mice in a C57BL/6J were all kept at conventional animal facility at the Faculty of Health and Medical Sciences, University of Copenhagen. Experiments were all approved and performed in accordance with the Danish ethical standards under ethical permission license 2018-15-0201-01572.

CD4 isolation

CD4$^+$ T cells were isolated from WT C57BL/6, CD4^{Cre}-Foxa1$^{fl/fl}$, and CD4^{Cre} mouse splenocytes by spleen mechanical rupture with a syringe plunger, followed by incubation with eBioscience 1× RBC Lysis Buffer (Thermo Fisher Scientific, catalog no. 00-4333-57) for 5 min at room temperature (RT). After the incubation time, cells were washed for 5300*g* and then filtered on a 70-μm cell strainer. CD4$^+$ T cells were purified from splenocytes using a CD4$^+$ T cells isolation kit (Miltenyi Biotec, CD4 T cell isolation kit, catalog no. 130-104-454) according to the manufacturer's instructions. Cells were plated in RPMI 1640 + L-glutamine (Thermo Fisher Scientific, 21875-034) supplemented with 10% fetal bovine serum, penicillin (100 U/ml), streptomycin (100 μg/ml), 10 mM Hepes, 50 μM 2-mercaptoethanol, 1 mM sodium pyruvate, and minimum essential medium nonessential amino acid solution (Gibco). After isolation, CD4$^+$ T cells were cultured in 96-well U-bottom plates for T_{reg} differentiation.

SepMate peripheral blood mononuclear cell protocol

Peripheral blood mononuclear cells (PBMCs) were obtained from the blood bank (Rigshospitalet, Copenhagen, Denmark) and isolated from the peripheral blood of healthy donors by density gradient centrifugation with Ficoll-Paque PLUS (VWR) through SepMate PBMC isolation tubes (STEMCELL Technologies). After 10 min of centrifuge at 1200*g*, lymphocytes were collected and washed two times at 8300*g* with 1× phosphate-buffered saline (PBS). After washing, CD4$^+$ T cells were isolated using CD4$^+$ T cells Isolation kit (MojoSort, Human CD4 T cell isolation kit, catalog no. 480009) and then cultured to induce T_{reg} differentiation.

T_{reg} differentiation

After the isolation, 2×10^5 CD4$^+$ T cells have been cultured in presence of IFNβ and TGFβ + interleukin-2 (IL-2) for 24 to 48 hours to induce FoxA1$^+$ and FoxP3$^+$ T_{regs}, respectively (Table 1). In some sets of experiments, cell cultures were treated with modulator of autophagy: Baf A1 (50 nM for 24 hours) (Sigma-Aldrich, B1793). To inhibit AMPK activity, compound C at final concentration of 5 and 10 mM (ENZO, BML-EI369-0005) has been used during 24 hours of T_{reg} differentiation. After 24 to 48 hours of culture, T_{regs} have been collected for the experiments.

Seahorse assay

After 48 hours of T_{reg} differentiation, iFoxA1$^+$ T_{regs} and iFoxP3$^+$ T_{regs} were transferred in 96-well cell culture V3 microplates in XF medium supplemented with glucose (10 mM), pyruvate (1 mM) and L-glutamine (2 mM). OCR real-time measurements were performed using an XFe-96 extracellular flux analyzer (Seahorse Agilent) under basal condition and in response to 1.5 μM oligomycin, 1.5 μM carbonylcyanide-4-(trifluoromethoxy)-phenylhydrazone, or 1 μM antimycin and rotenone (all from Mito Stress test kit, Agilent). Basal OXPHOS (before oligomycin addition) and ATP-linked OXPHOS (the difference between basal OCR and oligomycin-induced OCR) were calculated from the OCR profile as indices of mitochondrial respiratory function. Seahorse data were calculated by subtracting nonmitochondrial respiration from the OCR values, as indicated in the Seahorse XF Cell Mito Stress Test Equations & Example Calculations.

Table 1. Cytokines list.

	Mouse		Human	
	Catalog no.	Concentration	Catalog no.	Concentration
IFNβ	I9032-1VL, Sigma-Aldrich	1000 U/ml	11415-1, PBL Assay Science	1000 U/ml
TGFβ	7666-MB-005, R&D System	20 ng/ml	240-B-002, R&D System	20 ng/ml
IL-2	402-ML	2000 U/ml	202-IL-010, R&D System	2500 U/ml

In vitro suppression assay

To study the role of FoxA1 in the suppressive function of FoxA1$^+$ T_{regs}, we isolated splenocytes from $MOG_{35–55}$-induced EAE (experimental autoimmune encephalomyelitis) mice (*82*) and labeled them with CellTrace violet cell proliferation kit (catalog no. C34557). These cells served as responder T cells. The responder T cells were then treated with $MOG_{35–55}$ (50 μg/ml) for 72 hours before coculture with suppressor cells. iFoxA1$^+$ T_{regs} served as suppressor T cells were obtained from CD4$^+$ T cells isolated from C57BL/6J WT splenocytes as described above and then treated with IFNβ (100 U/ml), anti-CD3 (1 g/ml; 145-2C1), and anti-CD28 (10 g/ml; 37.51) for 48 hours before coculture with responder T cells. We then cocultured suppressor and responder T cells in a new culture plate at a 2:1 (suppressor:responder) ratio. For some experiments, suppressor T cells were obtained from CD4^{Cre} Foxa1$^{fl/fl}$ mice and/or upon silencing of PRKAG2.2 and BNIP3 by Accell siRNA. After 48 hours of cocultures, we analyzed the proliferation of responder cells by detecting CellTrace violet using FACS.

Proliferation and stability assays

To study the impact of PRKAG2.2 on iFoxA1$^+$ T_{reg} proliferation, we silenced PRKAG2.2 24 hours before the iFoxA1$^+$ T_{reg} differentiation. For the impact on iFoxA1$^+$ T_{regs} stability and maintenance, we silenced PRKAG2.2, 24 hours after the iFoxA1$^+$ T_{reg} differentiation. Cell proliferation and apoptosis data were analyzed using the CellTrace Violet Cell Proliferation Kit (catalog no. C34557) and annexin V–fluorescein isothiocyanate (FITC) (BD Pharmigen, 556419).

Real-time PCR

Total RNA was isolated using a QIAGEN kit (QIAGEN), reverse-transcribed into cDNA (iScript cDNA synthesis kit, catalog no. 1708891), and amplified and quantified by SYBR Green (Bio-Rad) detection. Relative mRNA expression was calculated using RPL13A gene expression as an endogenous (*83*). The primers used are listed in Table 2.

Mitochondrial analysis

Forty-eight hours after in vitro differentiation of iFoxA1$^+$ T_{regs} and iFoxP3$^+$ T_{regs}, to test mitochondrial mass, iFoxA1$^+$ T_{regs} and iFoxP3$^+$ T_{regs} were treated with MTG (50 nM) dye for 30 min at 37°C, and the signal was detected by flow cytometry. TMRE has been used for measuring mitochondrial membrane potential. iFoxA1$^+$ T_{regs} and iFoxP3$^+$ T_{regs} were treated with TMRE (50 nM) dye for 30 min at 37°C and analyzed by flow cytometry.

Table 2. Primers list.

Gene	Sequence
RPL13A forward	GCAGATCTTGAGGTTACGGA
RPL13A reverse	ATTGGGTTCACACCAGGA
PRKAG1 forward	CGAACTGGAGGAGCACAAGA
PRKAG1 reverse	CAGCATCAAACAAGCTGGCAT
PRKAG2 forward	TTGAAACGTGGAGGGAGTTGT
PRKAG2 reverse	TGCGTTCCCACTGATAGGGT
D-loop forward	AATCTACCATCCTCCGTGAAACC
D-loop reverse	TCAGTTTAGCTACCCCCAAGTTTAA

Mitophagy analysis by live-imaging confocal microscopy

CD4$^+$ T cells isolated from human donors and/or mice were treated with IFNβ or TGFβ + IL-2 for 48 hours to induce FoxA1$^+$ T_{reg} and FoxP3$^+$ T_{reg} differentiation, respectively. At the end of the treatment, live-imaging monitoring of mitophagy was achieved by attaching the cells on 96-well flat-bottom plates for microscopy (Greiner), with Cell-Tak Cell and Tissue Adhesive (Corning, 354240). At the end of the treatment, cells were stained for 10 min with 50 nM MTG, 200 nM LTR, and 10 μM Hoechst 33342 (Thermo Fisher Scientific), and then stained cells were washed once in PBS and replaced in full medium. As a positive control, 5 μM CCCP was added to the medium. The plate was then placed in the incubator chamber of the ImageXpress Micro Confocal High-Content Imaging System (Molecular Devices) at 37°C in an atmosphere of 5% CO_2. Pictures were captured every 5 min for 60 min. The analysis was performed on seven frames (30′ of acquisition) by Fiji ImageJ (*84*) using the plugin ComDet 0.5.5 (https://doi.org/10.5281/zenodo.4281064), adapting a previously reported protocol (*85*). The plugin finds and analyzes colocalization of bright intensity spots in images with heterogeneous background. The parameters used to calculate the colocalization were as follows: particles size of 3 pixels; intensity threshold = 3 for MTG and 5 for LTR. The colocalization was considered positive if the maximum distance between the center of two particles was 2 pixels. At least 30 cells deriving from independent experiments per experimental condition were analyzed. Results are reported both as total number and as an average number of colocalized mitochondria-lysosome/cell in 30 min.

Mitophagy analysis by Airyscan confocal microscopy

CD4$^+$ T cells isolated from human donors were treated with IFNβ or TGFβ + IL-2 for 48 hours to induce FoxA1$^+$ T_{reg} and FoxP3$^+$ T_{reg} differentiation, respectively. Cells were treated with BNIP3 siRNA for 72 hours. Cells were fixed with 4% paraformaldehyde and then transferred into 96-well plates for fluorescence microscopy coated with gelatin 0.5% (Sigma-Aldrich, G1393). Cells were incubated 5′ with a permeabilization solution (PBS/Triton X-100, 0.2%, v/v), blocked for 1 hour with a blocking solution (PBS/normal goat serum, 5%, v/v), and then incubated overnight with anti-LC3 (NanoTools) and anti-TOM20 (Santa Cruz Biotechnology) antibodies. Cells were then washed with cold PBS and incubated for 1 hour with fluorophore-conjugated secondary antibodies [Alexa Fluor 488 (AF488) and Alexa Fluor 568, respectively]. Nuclei were stained with Hoechst 33342 (Thermo Fisher Scientific). Confocal microscopy experiments were performed by using a Cell Discoverer 7 microscope (Zeiss) equipped with a LSM 900 and Airyscan-2 system. Images were acquired with a 50× water-immersion objective and acquired using 1.4× super-resolution function. For each field, ≥30 *z*-stacks of 0.2 μm were acquired. Images two-dimensional (2D) projections for representation and 3D reconstruction for the analysis were performed using Arivis Pro software (Zeiss). Mitophagy rate was calculated by counting the percentage of mitochondria overlapping for at least 10% (v/v) with LC3 particles in Baf-treated versus control-treated cells.

WB analysis

After T_{reg} differentiation, whole-cell extracts have been lysed in radioimmunoprecipitation assay and centrifuged. Cells were then sonicated, and the entire lysates were loaded. Anti-LC3B (L7543) and anti-vinculin (v4139) were purchased from Sigma-Aldrich. Anti-p62 (MBL-M162-3) was purchased from MBL. Opa1 (ab157457) was purchased from Abcam. AMPK substrate antibody sampler kit (#35277) was purchased from Cell Signaling Technology. PINK1 (ab23707) was purchased from Abcam. Parkin-Ser[65] (PA5-114616) was purchased from Thermo Fisher Scientific. The Odyssey system (LI-COR) was used for detection, and the ImageJ software was used for quantification. Vinculin has been used as a loading control. To detect OXPHOS complex assembly, we used an assembly-dependent total OXPHOS rodent antibody cocktail (Abcam, ab110413). The antibodies in the cocktail are against a subunit that is labile when its complex is not assembled. The samples were prepared following the manufacturer′s protocol.

RNA sequencing library preparation and analysis

Human buffy coats were collected from healthy donors aged 21 to 34 years. Four donors were used for each sample group (gender-matched, two male and two female donors in each group). As illustrated in (fig. S2A): From PBMCs, $CD4^+$ T cells were purified with the MojoSort Human $CD4^+$ T cells Isolation Kit (BioLegend, catalog no. 480009). Naïve $CD4^+$ T cells, and $FoxP3^+T_{reg}$ subsets eT_{regs}, and rT_{regs} were purified from the $CD4^+$ T cells on a FACSAria III. Cell subsets were sorted on the basis of exclusion of death cells using a live/dead violet staining (Thermo Fisher Scientific, catalog no. L34955), and surface markers CD4–phycoerythrin (PE)–Cy7 (BioLegend, catalog no. 317414), CD127-AF488 (BioLegend, catalog no. 351314), CD25-PE (BioLegend, catalog no. 356104), and CD45RA-AF647 (Invitrogen, catalog no. A51016) staining as indicated in the fig. S2A. Unstained cells were used as control to set the gate. Cells were sorted in "purity" mode using a 70-μm nozzle. Primary human T_{regs} were cultured and expanded for 14 days in TexMACS (Miltenyi Biotec, catalog no. 130-097-196) supplemented with 5% human AB serum (Sigma-Aldrich, catalog no. H4522-100ML), 0.01 mM β-mercaptoethanol (Sigma-Aldrich, catalog no. M3148), 1% penicillin-streptomycin (Gibco, catalog no. 15140-122), and 1% kanamycin sulfate (Thermo Fisher Scientific, catalog no. 15160054) using the T_{reg} expansion kit, human (Miltenyi Biotec, catalog no. 130-095-353) based on MACSiBead Particles preloaded with CD3 and CD28 antibodies, used in combination with recombinant human IL-2 (500 U/ml; R&D Systems, catalog no. 202-IL-010) that was added fresh to the medium each time.

$FoxP3^+rT_{regs}$ were resorted into rT_{reg} and aT_{reg} cell populations after expansion using the same sorting parameters to ensure high purity of rT_{regs}. Human $FoxP3^+iT_{regs}$ were polarized in vitro by stimulation of naïve $CD4^+$ T cells with α-CD3 (plate-bound; 5 μg/ml; Invitrogen, catalog no. 16-0037-81), α-CD28 (1 μg/ml; Invitrogen, catalog no. 16-0289-81), IL-2 (100 U/ml; R&D Systems, catalog no. 202-IL-010), and TGFβ (5 ng/ml; R&D Systems, catalog no. 240-B) as described (*86*) for 6 days. When indicated, human cells for RNA-seq were treated with recombinant hIFNβ (1000 U/ml; PBL Assay Science, catalog no. 11415-1) for 24 hours. Total RNA was extracted using the RNeasy mini kit (QIAGEN, catalog no. 74104). mRNA was prepared using oligo(dT) primers and reverse-transcribed (KAPA Biosystem, catalog no. KK2601). The resulting double-stranded DNA was tagmented (Illumina, catalog no. FC-131-1096) and ligated using Illumina sequencing adaptors (Illumina, catalog no. FC-131-2002), as detailed (*87*).

Libraries were pooled (1.6 pM) and sequenced using paired-end 75–base pair (bp) reads on an Illumina NextSeq500. At least four biological replicates (age- and gender-matched) were carried out for each sample. Preprocessing steps were conducted using Fastq Screen, FastQC, and Trimmomatic. Sequence reads were mapped to the *Homo sapiens* genome (version hg38) with STAR (version 2.6.0b-2), and, on average, 12 M reads aligned uniquely per library. Read counts for annotated features were computed by htseq-count using the hg38 *H. sapiens* gene annotation from iGenome. Pairwise comparison between two conditions was performed using DESeq2. All analyses were conducted using local Galaxy (BricwebGalaxy v19.05) (*88*). Heatmaps and volcano plot were constructed using DEBrowser in R (*89*). Filtration of low counts (fewer than four counts) and, when needed, batch-effect corrections were performed using Median Ratio Normalization (MRN) normalization and Combat batch correction. Venn diagram for comparing groups of genes was drawn using InteractiVenn (*90*). The histogram of the top 30 pathways was established representing the normalized enrichment score (NES) on GraphPad, based on the Reactome database and GO (Gene Ontology) (*91*). Parallel coordinate plots were used to plot enriched genes.

Chromatin immunoprecipitation sequencing

A total of 2×10^6 cells were used per ChIP-seq sample. The donors for ChIP-seq samples were the same as those for the RNA-seq. For human natural $FoxP3^+$ T_{reg} samples, two donors (one male and one female) were used for FoxP3 and FoxA1 immunoprecipitation, and two donors (one male and one female) were used for H3K4me3 and for human naïve $CD4^+$ T cells samples, two donors (one male and one female) were used for FoxA1 immunoprecipitation, and two donors (one male and one female) were used for H3K4me3. When specified, cells were treated with recombinant hIFNβ (1000 U/ml; PBL Assay Science, catalog no. 11415-1). Input samples for each condition were used as controls.

Cells were cross-linked with formaldehyde 1% for 7.5 min at RT. Cell lysis, cross-linking, and chromatin shearing were performed using the Covaris truCHIP protocol (Covaris, catalog no. 520154). Chromatin was sheared on an AFA focused ultrasonicator (M220) for 20 cycles at 4°C. Shearing efficiency of a minimum of 60% with a peak at 200 to 300 bp was verified using the Agilent Bioanalyzer High-Sensitivity DNA Analysis Kit (Agilent, catalog no. 5067-4626). The sheared chromatin was adjusted to a final NaCl concentration of 150 mM (for ion concentration) and Triton X-100 of 1% (to sequester the SDS) in the shearing buffer. Immunoprecipitation was performed on the basis of ChIP-IT PBMC (Active Motif, catalog no. 53042), using the following antibodies: FoxA1 (Abcam, catalog no. ab5089), H3K4me3 (Abcam, catalog no. ab8580), and T-box transcription factor (TBX21) (Santa Cruz Biotechnology, catalog no. sc-21749X).

After the immunoprecipitation, the chromatin was purified and reverse–cross-linked by adding ribonuclease A and proteinase K overnight at 65°C. DNA was purified using the MinElute PCR Purification Kit (QIAGEN, catalog no. 28006), followed by library preparation using the Ovation Ultralow System 183 V2, A01 (Nugen, catalog no. 0344NB-A01). For samples that contained less than 1 ng of DNA, the number of PCR amplification cycles

that were needed was determined by qPCR, according to the manufacturer's protocol. Libraries were pooled (1.8 pM) and sequenced by paired-end 75-bp reads on an Illumina NextSeq500. Preprocessing steps were performed using Fastq Screen, FastQC, and Trimmomatic. The reads were mapped to the human genome (GRCh38.p13, Gencode v33) using Bowtie, giving 6 to 12 M aligned reads per library. Peak calling was performed using MACS in local Galaxy (BricwebGalaxy v19.05) and Easeq (http://easeq.net) (*92*). Easeq was used for further analysis and figure preparation.

For differential analysis, the union peaks [peak calling criteria: $P < 1 \times 10^{-5}$, false discovery rate (FDR) $< 1 \times 10^{-5}$, $\log_2$fold diff > 2] between two conditions were generated for the replicates, and DESeq2 was used to analyze differential expression (DESeq2 criteria: $P < 0.05$ and $|\log_2 FC| > 0.5$). The peak view images throughout the manuscript are shown by merging biological replicates of mapping results.

Measurements of cellular ATP and ADP/ATP ratio

Cellular ATP levels were determined in iFoxA1$^+$ T_{regs} and iFoxP3$^+$ T_{regs} using ATP Assay Kit (Abcam, bioluminescent, ab65313) following the manufacturer's protocol. Briefly, iFoxA1$^+$ T_{regs} and iFoxP3$^+$ T_{regs} were differentiated for 48 hours, washed and harvested after mixing with nucleotide-releasing buffer, and incubated for 5 min at RT with gentle shaking. Then, 100 µl of prepared reaction mix was added to control wells, and the background luminescence was read (data A), then 50 µl of sample was added, and after 2 min, the luminescence was read (data B). To measure ADP levels in the cells, the samples were read again (data C), then added 10 µl of 1× ADP-converting enzyme, and read the samples again after approximately 2 min (data D). ADP/ATP ratio = [data D − data C]/[data B − data A].

siRNA knockdown of target genes

CD4$^+$ T cells isolated from human donor and/or mice were resuspended in Accell Delivery Media (Thermo Fisher Scientific, catalog no. B-005000-100), treated with Accell siRNA (PRKAG2.2 or BNIP3, where indicated in Results) and activated with ImmunoCult Human CD3/CD28 T cell activator (catalog no. 10991) for 72 hours. In some experiments, cells were treated with 1 mM PRKAG2.2 siRNA (Accell Human PRKAG2.2 custom siRNA: sense sequence, GAAGAGAGGACGCGAAUUAUU; antisense, UAAUUCGCGUCCUCUCUUCUU); or nontargeting control siRNA (Thermo Fisher Scientific, catalog no. D-001910-01-05) was added to each 100 µl of cells in Accell medium.

In other experiments, 1 mM Accell Smartpool siRNA BNIP3 (SO-3010691G) or nontargeting control siRNA (Thermo Fisher Scientific, catalog no. D-001910-01-05) was added to each 100 µl of cells in Accell medium for 72 hours in total. After 24 hours of siRNA treatment, CD4$^+$ T cells were treated with IFNb or TGFb + IL-2 for 48 hours to induce FoxA1$^+$ T_{reg} and FoxP3$^+$ T_{reg} differentiation and then were analyzed after 48 hours.

FACS staining

Cultured cells were collected and washed in FACS buffer (2% fetal bovine serum in PBS). Dead cells were excluded using live and dead marker (Invitrogen–Thermo Fisher Scientific) for 10 min at RT and then washed with 1× PBS. Surface markers have been stained with FACS antibodies for 30 min at RT (Table 1). For intracellular staining, cells were fixed and permeabilized using BD Cytofix/Cytoperm or using eBioscience Foxp3/transcription factor staining buffer set (catalog no. 00-5523-00) according to the manufacturer's instructions. After fixation and permeabilization, cells were washed for 5′ at 300*g* and stained for intracellular markers for 30 min at RT. Mouse and human panels are listed in Table 3. Human and mouse samples were acquired on the BD LSRFortessa X20 analyzer (BD Biosciences). FoxP3$^+$ T_{reg} gating strategy: CD4$^+$CD25$^+$FOXP3$^+$; FoxA1$^+$ T_{reg} gating strategy: CD4$^+$CD25$^-$CD2$^+$PD-L1$^+$FOXA1$^+$.

Statistical analysis

Statistical analysis was performed using the version 9.0 Prism software (GraphPad). One-way analysis of variance (ANOVA) was used to analyze Seahorse data CD4$^+$ T cells versus iFoxA1$^+$ T_{regs} and iFoxP3$^+$ T_{regs} and quantification of mitophagy in CD4$^+$ T cells,

Table 3. Mouse and human FACS antibody panel.

Mouse				Human			
Surface marker	**Parameter**	**Catalog number**	**Dilution**	**Surface marker**	**Parameter**	**Catalog number**	**Dilution**
Live/dead	UV 440		1:1000	Live/dead	UV 440		1:1000
CD4	APC-Cy7	100526, BioLegend	1:200	CD4	AF700	357418, BioLegend	1:200
CD2	Percp-Cy5.5	100116, BioLegend	1:200	CD2	BV711	300231, BioLegend	1:200
CD25	BV421	564370, BD	1:200	CD25	Percp-Cy5.5	356111, BioLegend	1:200
PDL1	Pe-Cy7	124314, BioLegend	1:50	PDL1	Pe-Cy7	558017, BD	1:50
FOXP3	PE	12-5773-82, eBioscience	1:50	FOXP3	PE	320107, BioLegend	1:50
FOXA1	AF647	612004, BioLegend	1:50	FOXA1	AF647	612004, BioLegend	1:50
PRKAG2	Second. AF 488*	#2536, Cell Signaling Technology	1:50	PRKAG2	Second AF488*	#2536, Cell Signaling Technology	1:50
LC3B	PE	#8899, Cell Signaling Technology	1:50	LC3B	PE	#8899, Cell Signaling Technology	1:50

*AF488 goat anti-rabbit Invitrogen (A11034) immunoglobulin G.

iFoxA1$^+$ T_{regs}, and iFoxP3$^+$ T_{regs} acquired in live by ImageXpress microconfocal microscope. A two-tailed unpaired Student's *t* test was used to analyze MTG and TMRE to compare CD4$^+$ T cells versus iFoxA1$^+$ T_{regs}. Two-way ANOVA was performed for in vitro analysis in which we compared CD4^{Cre} versus CD4^{Cre} Foxa1$^{fl/fl}$ mice upon TGFβ/IFNβ treatment. One-way ANOVA was applied to compare treatment with autophagy modulators and upon silencing. Every in vitro assay was performed in duplicate or triplicate, when possible. The number of repetitions is indicated in the figure legend for all experiments. In all graphs, bars show means ± SEM. In all tests, $P < 0.05$ was considered statistically significant.

Supplementary Materials

This PDF file includes:
Figs. S1 to S5
Legends for files S1 to S6

Other Supplementary Material for this manuscript includes the following:
Files S1 to S6

REFERENCES AND NOTES

1. F. Powrie, R. Correa-Oliveira, S. Mauze, R. L. Coffman, Regulatory interactions between CD45RBhigh and CD45RBlow CD4+ T cells are important for the balance between protective and pathogenic cell-mediated immunity. *J. Exp. Med.* **179**, 589–600 (1994).
2. S. Sakaguchi, N. Sakaguchi, M. Asano, M. Itoh, M. Toda, Immunologic self-tolerance maintained by activated T cells expressing IL-2 receptor alpha-chains (CD25). Breakdown of a single mechanism of self-tolerance causes various autoimmune diseases. *J. Immunol.* **155**, 1151–1164 (1995).
3. A. Y. Rudensky, Regulatory T cells and Foxp3. *Immunol. Rev.* **241**, 260–268 (2011).
4. J. D. Fontenot, M. A. Gavin, A. Y. Rudensky, Foxp3 programs the development and function of CD4$^+$CD25$^+$ regulatory T cells. *Nat. Immunol.* **4**, 330–336 (2003).
5. S. Hori, T. Nomura, S. Sakaguchi, Pillars article: Control of regulatory T cell development by the transcription factor Foxp3. Science 2003. 299: 1057-1061. *J. Immunol.* **198**, 981–985 (2017).
6. Y. Y. Wan, R. A. Flavell, 'Yin-Yang' functions of transforming growth factor-β and T regulatory cells in immune regulation. *Immunol. Rev.* **220**, 199–213 (2007).
7. J. Shimizu, S. Yamazaki, S. Sakaguchi, Induction of tumor immunity by removing CD25 +CD4+ T cells: A common basis between tumor immunity and autoimmunity. *J. Immunol.* **163**, 5211–5218 (1999).
8. T. Takahashi, T. Tagami, S. Yamazaki, T. Uede, J. Shimizu, N. Sakaguchi, T. W. Mak, S. Sakaguchi, Immunologic self-tolerance maintained by CD25$^+$CD4$^+$ regulatory T cells constitutively expressing cytotoxic T lymphocyte-associated antigen 4. *J. Exp. Med.* **192**, 303–310 (2000).
9. Q. Chen, Y. C. Kim, A. Laurence, G. A. Punkosdy, E. M. Shevach, IL-2 controls the stability of Foxp3 expression in TGF-β-induced Foxp3+ T cells in vivo. *J. Immunol.* **186**, 6329–6337 (2011).
10. Y. Liu, R. Carlsson, M. Comabella, J. Wang, M. Kosicki, B. Carrion, M. Hasan, X. Wu, X. Montalban, M. H. Dziegiel, F. Sellebjerg, P. S. Sorensen, K. Helin, S. Issazadeh-Navikas, FoxA1 directs the lineage and immunosuppressive properties of a novel regulatory T cell population in EAE and MS. *Nat. Med.* **20**, 272–282 (2014).
11. J. Liang, C. Tian, Y. Zeng, Q. Yang, Y. Liu, Y. Liu, J. Wu, Y. Hu, F. Gu, K. Zhang, Y. Wang, Y. Zhang, L. Liu, FOXA1$^+$ regulatory T cells: A novel T cell subset that suppresses antitumor immunity in lung cancer. *Biochem. Biophys. Res. Commun.* **514**, 308–315 (2019).
12. Y. Liu, A. Marin, P. Ejlerskov, L. M. Rasmussen, M. Prinz, S. Issazadeh-Navikas, Neuronal IFN-beta-induced PI3K/Akt-FoxA1 signalling is essential for generation of FoxA1$^+$ T_{reg} cells. *Nat. Commun.* **8**, 14709 (2017).
13. S. Roy, Z. A. Rizvi, A. Awasthi, Metabolic checkpoints in differentiation of helper T cells in tissue inflammation. *Front. Immunol.* **9**, 3036 (2018).
14. C. S. Palmer, M. Ostrowski, B. Balderson, N. Christian, S. M. Crowe, Glucose metabolism regulates T cell activation, differentiation, and functions. *Front. Immunol.* **6**, 1 (2015).
15. N. J. MacIver, R. D. Michalek, J. C. Rathmell, Metabolic regulation of T lymphocytes. *Annu. Rev. Immunol.* **31**, 259–283 (2013).
16. R. D. Michalek, V. A. Gerriets, S. R. Jacobs, A. N. Macintyre, N. J. MacIver, E. F. Mason, S. A. Sullivan, A. G. Nichols, J. C. Rathmell, Cutting edge: Distinct glycolytic and lipid oxidative metabolic programs are essential for effector and regulatory CD4+ T cell subsets. *J. Immunol.* **186**, 3299–3303 (2011).
17. Y. Yang, A. A. Sauve, NAD$^+$ metabolism: Bioenergetics, signaling and manipulation for therapy. *Biochim. Biophys. Acta* **1864**, 1787–1800 (2016).
18. J. M. Moreau, M. Velegraki, C. Bolyard, M. D. Rosenblum, Z. Li, Transforming growth factor–β1 in regulatory T cell biology. *Sci Immunol* **7**, eabi4613 (2022).
19. A. Angelin, L. Gil-de-Gomez, S. Dahiya, J. Jiao, L. Guo, M. H. Levine, Z. Wang, W. J. Quinn 3rd, P. K. Kopinski, L. Wang, T. Akimova, Y. Liu, T. R. Bhatti, R. Han, B. L. Laskin, J. A. Baur, I. A. Blair, D. C. Wallace, W. W. Hancock, U. H. Beier, Foxp3 reprograms T cell metabolism to function in Low-glucose, high-lactate environments. *Cell Metab.* **25**, 1282–1293.e7 (2017).
20. U. H. Beier, A. Angelin, T. Akimova, L. Wang, Y. Liu, H. Xiao, M. A. Koike, S. A. Hancock, T. R. Bhatti, R. Han, J. Jiao, S. C. Veasey, C. A. Sims, J. A. Baur, D. C. Wallace, W. W. Hancock, Essential role of mitochondrial energy metabolism in Foxp3$^+$ T-regulatory cell function and allograft survival. *FASEB J.* **29**, 2315–2326 (2015).
21. S. Herzig, R. J. Shaw, AMPK: Guardian of metabolism and mitochondrial homeostasis. *Nat. Rev. Mol. Cell Biol.* **19**, 121–135 (2018).
22. J. A. Shyer, R. A. Flavell, W. Bailis, Metabolic signaling in T cells. *Cell Res.* **30**, 649–659 (2020).
23. P. C. Cheung, I. P. Salt, S. P. Davies, D. G. Hardie, D. Carling, Characterization of AMP-activated protein kinase γ-subunit isoforms and their role in AMP binding. *Biochem. J.* **346**, 659–669 (2000).
24. T. Lang, L. Yu, Q. Tu, J. Jiang, Z. Chen, Y. Xin, G. Liu, S. Zhao, Molecular cloning, genomic organization, and mapping of PRKAG2, a heart abundant γ2 subunit of 5′-AMP-activated protein kinase, to human chromosome 7q36. *Genomics* **70**, 258–263 (2000).
25. M. M. Mihaylova, R. J. Shaw, The AMPK signalling pathway coordinates cell growth, autophagy and metabolism. *Nat. Cell Biol.* **13**, 1016–1023 (2011).
26. D. Wu, D. E. Sanin, B. Everts, Q. Chen, J. Qiu, M. D. Buck, A. Patterson, A. M. Smith, C. H. Chang, Z. Liu, M. N. Artyomov, E. L. Pearce, M. Cella, E. J. Pearce, Type 1 interferons induce changes in core metabolism that are critical for immune function. *Immunity* **44**, 1325–1336 (2016).
27. J. Magalhaes, E. Tresse, P. Ejlerskov, E. Hu, Y. Liu, A. Marin, A. Montalant, L. Satriano, C. F. Rundsten, E. M. M. Carlsen, R. Rydbirk, A. Sharifi-Zarchi, J. B. Andersen, S. Aznar, T. Brudek, K. Khodosevich, M. Prinz, J. M. Perrier, M. Sharma, T. Gasser, S. Issazadeh-Navikas, PIAS2-mediated blockade of IFN-β signaling: A basis for sporadic Parkinson disease dementia. *Mol. Psychiatry* **26**, 6083–6099 (2021).
28. E. Tresse, L. Riera-Ponsati, E. Jaberi, W. Q. G. Sew, K. Ruscher, S. Issazadeh-Navikas, IFN-β rescues neurodegeneration by regulating mitochondrial fission via STAT5, PGAM5, and Drp1. *EMBO J.* **40**, e106868 (2021).
29. E. Tresse, J. Marturia-Navarro, W. Q. G. Sew, M. Cisquella-Serra, E. Jaberi, L. Riera-Ponsati, N. Fauerby, E. Hu, O. Kretz, S. Aznar, S. Issazadeh-Navikas, Mitochondrial DNA damage triggers spread of Parkinson's disease-like pathology. *Mol. Psychiatry*, (2023). 10.1038/s41380-023-02251-4
30. A. Subramanian, P. Tamayo, V. K. Mootha, S. Mukherjee, B. L. Ebert, M. A. Gillette, A. Paulovich, S. L. Pomeroy, T. R. Golub, E. S. Lander, J. P. Mesirov, Gene set enrichment analysis: A knowledge-based approach for interpreting genome-wide expression profiles. *Proc. Natl. Acad. Sci. U.S.A.* **102**, 15545–15550 (2005).
31. K. T. Bashour, A. Gondarenko, H. Chen, K. Shen, X. Liu, M. Huse, J. C. Hone, L. C. Kam, CD28 and CD3 have complementary roles in T-cell traction forces. *Proc. Natl. Acad. Sci. U.S.A.* **111**, 2241–2246 (2014).
32. K. T. Bashour, J. Tsai, K. Shen, J. H. Lee, E. Sun, M. C. Milone, M. L. Dustin, L. C. Kam, Cross talk between CD3 and CD28 is spatially modulated by protein lateral mobility. *Mol. Cell. Biol.* **34**, 955–964 (2014).
33. M. Huttemann, I. Lee, A. Pecinova, P. Pecina, K. Przyklenk, J. W. Doan, Regulation of oxidative phosphorylation, the mitochondrial membrane potential, and their role in human disease. *J. Bioenerg. Biomembr.* **40**, 445–456 (2008).
34. E. A. Liberman, V. P. Topaly, L. M. Tsofina, A. A. Jasaitis, V. P. Skulachev, Mechanism of coupling of oxidative phosphorylation and the membrane potential of mitochondria. *Nature* **222**, 1076–1078 (1969).
35. G. Twig, O. S. Shirihai, The interplay between mitochondrial dynamics and mitophagy. *Antioxid. Redox Signal.* **14**, 1939–1951 (2011).
36. R. J. Youle, D. P. Narendra, Mechanisms of mitophagy. *Nat. Rev. Mol. Cell Biol.* **12**, 9–14 (2011).
37. I. Tanida, T. Ueno, E. Kominami, LC3 conjugation system in mammalian autophagy. *Int. J. Biochem. Cell Biol.* **36**, 2503–2518 (2004).
38. D. J. Klionsky, A. K. Abdel-Aziz, S. Abdelfatah, M. Abdellatif, A. Abdoli, S. Abel, H. Abeliovich, M. H. Abildgaard, Y. P. Abudu, A. Acevedo-Arozena, I. E. Adamopoulos, K. Adeli, T. E. Adolph, A. Adornetto, E. Aflaki, G. Agam, A. Agarwal, B. B. Aggarwal, M. Agnello, P. Agostinis, J. N. Agrewala, A. Agrotis, P. V. Aguilar, S. T. Ahmad, Z. M. Ahmed, U. Ahumada-Castro,

S. Aits, S. Aizawa, Y. Akkoc, T. Akoumianaki, H. A. Akpinar, A. M. Al-Abd, L. Al-Akra, A. Al-Gharaibeh, M. A. Alaoui-Jamali, S. Alberti, E. Alcocer-Gomez, C. Alessandri, M. Ali, M. A. A. Al-Bari, S. Aliwaini, J. Alizadeh, E. Almacellas, A. Almasan, A. Alonso, G. D. Alonso, N. Altan-Bonnet, D. C. Altieri, E. M. C. Alvarez, S. Alves, C. A. da Costa, M. M. Alzaharna, M. Amadio, C. Amantini, C. Amaral, S. Ambrosio, A. O. Amer, V. Ammanathan, Z. An, S. U. Andersen, S. A. Andrabi, M. Andrade-Silva, A. M. Andres, S. Angelini, D. Ann, U. C. Anozie, M. Y. Ansari, P. Antas, A. Antebi, Z. Anton, T. Anwar, L. Apetoh, N. Apostolova, T. Araki, Y. Araki, K. Arasaki, W. L. Araujo, J. Araya, C. Arden, M. A. Arevalo, S. Arguelles, E. Arias, J. Arikkath, H. Arimoto, A. R. Ariosa, D. Armstrong-James, L. Arnaune-Pelloquin, A. Aroca, D. S. Arroyo, I. Arsov, R. Artero, D. M. L. Asaro, M. Aschner, M. Ashrafizadeh, O. Ashur-Fabian, A. G. Atanasov, A. K. Au, P. Auberger, H. W. Auner, L. Aurelian, R. Autelli, L. Avagliano, Y. Avalos, S. Aveic, C. A. Aveleira, T. Avin-Wittenberg, Y. Aydin, S. Ayton, S. Ayyadevara, M. Azzopardi, M. Baba, J. M. Backer, S. K. Backues, D. H. Bae, O. N. Bae, S. H. Bae, E. H. Baehrecke, A. Baek, S. H. Baek, G. Bagetta, A. Bagniewska-Zadworna, H. Bai, J. Bai, X. Bai, Y. Bai, N. Bairagi, S. Baksi, T. Balbi, C. T. Baldari, W. Balduini, A. Ballabio, M. Ballester, S. Balazadeh, R. Balzan, R. Bandopadhyay, S. Banerjee, S. Banerjee, A. Banreti, Y. Bao, M. S. Baptista, A. Baracca, C. Barbati, A. Bargiela, D. Barila, P. G. Barlow, S. J. Barmada, E. Barreiro, G. E. Barreto, J. Bartek, B. Bartel, A. Bartolome, G. R. Barve, S. H. Basagoudanavar, D. C. Bassham, R. C. Bast Jr., A. Basu, H. Batoko, I. Batten, E. E. Baulieu, B. L. Baumgarner, J. Bayry, R. Beale, I. Beau, F. Beaumatin, L. R. G. Bechara, G. R. Beck Jr., M. F. Beers, J. Begun, C. Behrends, G. M. N. Behrens, R. Bei, E. Bejarano, S. Bel, C. Behl, A. Belaid, N. Belgareh-Touze, C. Bellarosa, F. Belleudi, M. B. Perez, R. Bello-Morales, J. S. O. Beltran, S. Beltran, D. M. Benbrook, M. Bendorius, B. A. Benitez, I. Benito-Cuesta, J. Bensalem, M. W. Berchtold, S. Berezowska, D. Bergamaschi, M. Bergami, A. Bergmann, L. Berliocchi, C. Berlioz-Torrent, A. Bernard, L. Berthoux, C. G. Besirli, S. Besteiro, V. M. Betin, R. Beyaert, J. S. Bezbradica, K. Bhaskar, I. Bhatia-Kissova, R. Bhattacharya, S. Bhattacharya, S. Bhattacharyya, M. S. Bhuiyan, S. K. Bhutia, L. Bi, X. Bi, T. J. Biden, K. Bijian, V. A. Billes, N. Binart, C. Bincoletto, A. B. Birgisdottir, G. Bjorkoy, G. Blanco, A. Blas-Garcia, J. Blasiak, R. Blomgran, K. Blomgren, J. S. Blum, E. Boada-Romero, M. Boban, K. Boesze-Battaglia, P. Boeuf, B. Boland, P. Bomont, P. Bonaldo, S. R. Bonam, L. Bonfili, J. S. Bonifacino, B. A. Boone, M. D. Bootman, M. Bordi, C. Borner, B. C. Bornhauser, G. Borthakur, J. Bosch, S. Bose, L. M. Botana, J. Botas, C. M. Boulanger, M. E. Boulton, M. Bourdenx, B. Bourgeois, N. M. Bourke, G. Bousquet, P. Boya, P. V. Bozhkov, L. H. M. Bozi, T. O. Bozkurt, D. E. Brackney, C. H. Brandts, R. J. Braun, G. H. Braus, R. Bravo-Sagua, J. M. B.-S. Pedro, P. Brest, M. A. Bringer, A. Briones-Herrera, V. C. Broaddus, P. Brodersen, J. L. Brodsky, S. L. Brody, P. G. Bronson, J. M. Bronstein, C. N. Brown, R. E. Brown, P. C. Brum, J. H. Brumell, N. Brunetti-Pierri, D. Bruno, R. J. Bryson-Richardson, C. Bucci, C. Buchrieser, M. Bueno, L. E. Buitrago-Molina, S. Buraschi, S. Buch, J. R. Buchan, E. M. Buckingham, H. Budak, M. Budini, G. Bultynck, F. Burada, J. R. Burgoyne, M. I. Buron, V. Bustos, S. Buttner, E. Butturini, A. Byrd, I. Cabas, S. Cabrera-Benitez, K. Cadwell, J. Cai, L. Cai, Q. Cai, M. Cairo, J. A. Calbet, G. A. Caldwell, K. A. Caldwell, J. A. Call, R. Calvani, A. C. Calvo, M. C.-R. Barrera, N. O. Camara, J. H. Camonis, N. Camougrand, M. Campanella, E. M. Campbell, F. X. Campbell-Valois, S. Campello, I. Campesi, J. C. Campos, O. Camuzard, J. Cancino, D. C. de Almeida, L. Canesi, I. Caniggia, B. Canonico, C. Canti, B. Cao, M. Caraglia, B. Carames, E. H. Carchman, E. Cardenal-Munoz, C. Cardenas, L. Cardenas, S. M. Cardoso, J. S. Carew, G. F. Carle, G. Carleton, S. Carloni, D. Carmona-Gutierrez, L. A. Carneiro, O. Carnevali, J. M. Carosi, S. Carra, A. Carrier, L. Carrier, B. Carroll, A. B. Carter, A. N. Carvalho, M. Casanova, C. Casas, J. Casas, C. Cassioli, E. F. Castillo, K. Castillo, S. Castillo-Lluva, F. Castoldi, M. Castori, A. F. Castro, M. Castro-Caldas, J. Castro-Hernandez, S. Castro-Obregon, S. D. Catz, C. Cavadas, F. Cavaliere, G. Cavallini, M. Cavinato, M. L. Cayuela, P. C. Rica, V. Cecarini, F. Cecconi, M. Cechowska-Pasko, S. Cenci, V. Ceperuelo-Mallafre, J. J. Cerqueira, J. M. Cerutti, D. Cervia, V. B. Cetintas, S. Cetrullo, H. J. Chae, A. S. Chagin, C. Y. Chai, G. Chakrabarti, O. Chakrabarti, T. Chakraborty, T. Chakraborty, M. Chami, G. Chamilos, D. W. Chan, E. Y. W. Chan, E. D. Chan, H. Y. E. Chan, H. H. Chan, H. Chan, M. T. V. Chan, Y. S. Chan, P. K. Chandra, C. P. Chang, C. Chang, H. C. Chang, K. Chang, J. Chao, T. Chapman, N. Charlet-Berguerand, S. Chatterjee, S. K. Chaube, A. Chaudhary, S. Chauhan, E. Chaum, F. Checler, M. E. Cheetham, C. S. Chen, G. C. Chen, J. F. Chen, L. L. Chen, L. Chen, L. Chen, M. Chen, M. K. Chen, N. Chen, Q. Chen, R. H. Chen, S. Chen, W. Chen, W. Chen, X. M. Chen, X. W. Chen, X. Chen, Y. Chen, Y. G. Chen, Y. Chen, Y. Chen, Y. J. Chen, Y. Q. Chen, Z. S. Chen, Z. Chen, Z. H. Chen, Z. J. Chen, Z. Chen, H. Cheng, J. Cheng, S. Y. Cheng, W. Cheng, X. Cheng, X. T. Cheng, Y. Cheng, Z. Cheng, Z. Chen, H. Cheong, J. K. Cheong, B. V. Chernyak, S. Cherry, C. F. R. Cheung, C. H. A. Cheung, K. H. Cheung, E. Chevet, R. J. Chi, A. K. S. Chiang, F. Chiaradonna, R. Chiarelli, M. Chiariello, N. Chica, S. Chiocca, M. Chiong, S. H. Chiou, A. I. Chiramel, V. Chiurchiu, D. H. Cho, S. K. Choe, A. M. K. Choi, M. E. Choi, K. R. Choudhury, N. S. Chow, C. T. Chu, J. P. Chua, J. J. E. Chua, H. Chung, K. P. Chung, S. Chung, S. H. Chung, Y. L. Chung, V. Cianfanelli, I. A. Ciechomska, M. Cifuentes, L. Cinque, S. Cirak, M. Cirone, M. J. Clague, R. Clarke, E. Clementi, E. M. Coccia, P. Codogno, E. Cohen, M. M. Cohen, T. Colasanti, F. Colasuonno, R. A. Colbert, A. Colell, M. Colic, N. S. Coll, M. O. Collins, M. I. Colombo, D. A. Colon-Ramos, L. Combaret, S. Comincini, M. R. Cominetti, A. Consiglio, A. Conte, F. Conti, V. R. Contu, M. R. Cookson, K. M. Coombs, I. Coppens, M. T. Corasaniti, D. P. Corkery, N. Cordes, K. Cortese, M. D. C. Costa, S. Costantino, P. Costelli, A. Coto-Montes, P. J. Crack, J. L. Crespo, A. Criollo, V. Crippa, R. Cristofani, T. Csizmadia, A. Cuadrado, B. Cui, J. Cui, Y. Cui, Y. Cui, E. Culetto, A. C. Cumino, A. V. Cybulsky, M. J. Czaja, S. J. Czuczwar, S. D'Adamo, M. D'Amelio, D. D'Arcangelo, A. C. D'Lugos, G. D'Orazi, J. A. da Silva, H. S. Dafsari, R. K. Dagda, Y. Dagdas, M. Daglia, X. Dai, Y. Dai, Y. Dai, J. D. Col, P. Dalhaimer, L. D. Valle, T. Dallenga, G. Dalmasso, M. Damme, I. Dando, N. P. Dantuma, A. L. Darling, H. Das, S. Dasarathy, S. K. Dasari, S. Dash, O. Daumke, A. N. Dauphinee, J. S. Davies, V. A. Davila, R. J. Davis, T. Davis, S. D. Naidu, F. De Amicis, K. De Bosscher, F. De Felice, L. De Franceschi, C. De Leonibus, M. G. de Mattos Barbosa, G. R. Y. De Meyer, A. De Milito, C. De Nunzio, C. De Palma, M. De Santi, C. De Virgilio, D. De Zio, J. Debnath, B. J. DeBosch, J. P. Decuypere, M. A. Deehan, G. Deflorian, J. DeGregori, B. Dehay, G. Del Rio, J. R. Delaney, L. M. D. Delbridge, E. Delorme-Axford, M. V. Delpino, F. Demarchi, V. Dembitz, N. D. Demers, H. Deng, Z. Deng, J. Dengjel, P. Dent, D. Denton, M. L. DePamphilis, C. J. Der, V. Deretic, A. Descoteaux, L. Devis, S. Devkota, O. Devuyst, G. Dewson, M. Dharmasivam, R. Dhiman, D. di Bernardo, M. Di Cristina, F. Di Domenico, P. Di Fazio, A. Di Fonzo, G. Di Guardo, G. M. Di Guglielmo, L. Di Leo, C. Di Malta, A. Di Nardo, M. Di Rienzo, F. Di Sano, G. Diallinas, J. Diao, G. Diaz-Araya, I. Diaz-Laviada, J. M. Dickinson, M. Diederich, M. Dieude, I. Dikic, S. Ding, W. X. Ding, L. Dini, J. Dinic, M. Dinic, A. T. Dinkova-Kostova, M. S. Dionne, J. H. W. Distler, A. Diwan, I. M. C. Dixon, M. Djavaheri-Mergny, I. Dobrinski, O. Dobrovinskaya, R. Dobrowolski, R. C. J. Dobson, J. Dokic, S. D. Emre, M. Donadelli, B. Dong, X. Dong, Z. Dong, G. W. D. Ii, V. Dotsch, H. Dou, J. Dou, M. Dowaidar, S. Dridi, L. Drucker, A. Du, C. Du, G. Du, H. N. Du, L. L. Du, A. du Toit, S. B. Duan, X. Duan, S. P. Duarte, A. Dubrovska, E. A. Dunlop, N. Dupont, R. V. Duran, B. S. Dwarakanath, S. A. Dyshlovoy, D. Ebrahimi-Fakhari, L. Eckhart, C. L. Edelstein, T. Efferth, E. Eftekharpour, L. Eichinger, N. Eid, T. Eisenberg, N. T. Eissa, S. Eissa, M. Ejarque, A. El Andaloussi, N. El-Hage, S. El-Naggar, A. M. Eleuteri, E. S. El-Shafey, M. Elgendy, A. G. Eliopoulos, M. M. Elizalde, P. M. Elks, H. P. Elsasser, E. S. Elsherbiny, B. M. Emerling, N. C. T. Emre, C. H. Eng, N. Engedal, A. M. Engelbrecht, A. S. T. Engelsen, J. M. Enserink, R. Escalante, A. Esclatine, M. Escobar-Henriques, E. L. Eskelinen, L. Espert, M. O. Eusebio, G. Fabrias, C. Fabrizi, A. Facchiano, F. Facchiano, B. Fadeel, C. Fader, A. C. Faesen, W. D. Fairlie, A. Falco, B. H. Falkenburger, D. Fan, J. Fan, Y. Fan, E. F. Fang, Y. Fang, Y. Fang, M. Fanto, T. Farfel-Becker, M. Faure, G. Fazeli, A. O. Fedele, A. M. Feldman, D. Feng, J. Feng, L. Feng, Y. Feng, Y. Feng, W. Feng, T. F. Araujo, T. A. Ferguson, A. F. Fernandez, J. C. Fernandez-Checa, S. Fernandez-Veledo, A. R. Fernie, A. W. Ferrante Jr., A. Ferraresi, M. F. Ferrari, J. C. B. Ferreira, S. Ferro-Novick, A. Figueras, R. Filadi, N. Filigheddu, E. Filippi-Chiela, G. Filomeni, G. M. Fimia, V. Fineschi, F. Finetti, S. Finkbeiner, E. A. Fisher, P. B. Fisher, F. Flamigni, S. J. Fliesler, T. H. Flo, I. Florance, O. Florey, T. Florio, E. Fodor, C. Follo, E. A. Fon, A. Forlino, F. Fornai, P. Fortini, A. Fracassi, A. Fraldi, B. Franco, R. Franco, F. Franconi, L. B. Frankel, S. L. Friedman, L. F. Frohlich, G. Fruhbeck, J. M. Fuentes, Y. Fujiki, N. Fujita, Y. Fujiwara, M. Fukuda, S. Fulda, L. Furic, N. Furuya, C. Fusco, M. U. Gack, L. Gaffke, S. Galadari, A. Galasso, M. F. Galindo, S. G. Kankanamalage, L. Galluzzi, V. Galy, N. Gammoh, B. Gan, I. G. Ganley, F. Gao, H. Gao, M. Gao, P. Gao, S. J. Gao, W. Gao, X. Gao, A. Garcera, M. N. Garcia, V. E. Garcia, F. G.-D. Portillo, V. Garcia-Escudero, A. Garcia-Garcia, M. Garcia-Macia, D. Garcia-Moreno, C. Garcia-Ruiz, P. Garcia-Sanz, A. D. Garg, R. Gargini, T. Garofalo, R. F. Garry, N. C. Gassen, D. Gatica, L. Ge, W. Ge, R. Geiss-Friedlander, C. Gelfi, P. Genschik, I. E. Gentle, V. Gerbino, C. Gerhardt, K. Germain, M. Germain, D. A. Gewirtz, E. G. Afshar, S. Ghavami, A. Ghigo, M. Ghosh, G. Giamas, C. Giampietri, A. Giatromanolaki, G. E. Gibson, S. B. Gibson, V. Ginet, E. Giniger, C. Giorgi, H. Girao, S. E. Girardin, M. Giridharan, S. Giuliano, C. Giulivi, S. Giuriato, J. Giustiniani, A. Gluschko, V. Goder, A. Goginashvili, J. Golab, D. C. Goldstone, A. Golebiewska, L. R. Gomes, R. Gomez, R. Gomez-Sanchez, M. C. Gomez-Puerto, R. Gomez-Sintes, Q. Gong, F. M. Goni, J. Gonzalez-Gallego, T. Gonzalez-Hernandez, R. A. Gonzalez-Polo, J. A. Gonzalez-Reyes, P. Gonzalez-Rodriguez, I. S. Goping, M. S. Gorbatyuk, N. V. Gorbunov, K. Gorgulu, R. M. Gorojod, S. M. Gorski, S. Goruppi, C. Gotor, R. A. Gottlieb, I. Gozes, D. Gozuacik, M. Graef, M. H. Graler, V. Granatiero, D. Grasso, J. P. Gray, D. R. Green, A. Greenhough, S. L. Gregory, E. F. Griffin, M. W. Grinstaff, F. Gros, C. Grose, A. S. Gross, F. Gruber, P. Grumati, T. Grune, X. Gu, J. L. Guan, C. M. Guardia, K. Guda, F. Guerra, C. Guerri, P. Guha, C. Guillen, S. Gujar, A. Gukovskaya, I. Gukovsky, J. Gunst, A. Gunther, A. R. Guntur, C. Guo, C. Guo, H. Guo, L. W. Guo, M. Guo, P. Gupta, S. K. Gupta, S. Gupta, V. B. Gupta, V. Gupta, A. B. Gustafsson, D. D. Gutterman, B. R. H. A. Haapasalo, J. E. Haber, A. Hac, S. Hadano, A. J. Hafren, M. Haidar, B. S. Hall, G. Hallden, A. Hamacher-Brady, A. Hamann, M. Hamasaki, W. Han, M. Hansen, P. I. Hanson, Z. Hao, M. Harada, L. Harhaji-Trajkovic, N. Hariharan, N. Haroon, J. Harris, T. Hasegawa, N. H. Nagoor, J. A. Haspel, V. Haucke, W. D. Hawkins, B. A. Hay, C. M. Haynes, S. B. Hayrabedyan, T. S. Hays, C. He, Q. He, R. R. He, Y. W. He, Y. Y. He, Y. Heakal, A. M. Heberle, J. F. Hejtmancik, G. V. Helgason, V. Henkel, M. Herb, A. Hergovich, A. Herman-Antosiewicz, A. Hernandez, C. Hernandez, S. Hernandez-Diaz, V. Hernandez-Gea, A. Herpin, J. Herreros, J. H. Hervas, D. Hesselson, C. Hetz, V. T. Heussler, Y. Higuchi, S. Hilfiker, J. A. Hill, W. S. Hlavacek, E. A. Ho, I. H. T. Ho, P. W. Ho, S. L. Ho, W. Y. Ho, G. A. Hobbs, M. Hochstrasser, P. H. M. Hoet, D. Hofius, P. Hofman, A. Hohn, C. I. Holmberg, J. R. Hombrebueno, C. H. Y.-R. Hong, L. V. Hooper, T. Hoppe, R. Horos, Y. Hoshida, I. L. Hsin, H. Y. Hsu, B. Hu, D. Hu, L. F. Hu, M. C. Hu, R. Hu, W. Hu, Y. C. Hu, Z. W. Hu, F. Hua, J. Hua, Y. Hua, C. Huan, C. Huang, C. Huang, C. Huang, C. Huang, H. Huang, K. Huang, M. L. H. Huang, R. Huang, S. Huang, T. Huang, X. Huang, Y. J. Huang, T. B. Huber, V. Hubert, C. A. Hubner, S. M. Hughes, W. E. Hughes, M. Humbert, G. Hummer, J. H. Hurley, S. Hussain, S. Hussain, P. J. Hussey, M. Hutabarat, H. Y. Hwang, S. Hwang, A. Ieni, F. Ikeda, Y. Imagawa, Y. Imai, C. Imbriano, M. Imoto, D. M. Inman, K. Inoki, J. Iovanna, R. V. Iozzo, G. Ippolito, J. E. Irazoqui, P. Iribarren, M. Ishaq, M. Ishikawa,

N. Ishimwe, C. Isidoro, N. Ismail, S. Issazadeh-Navikas, E. Itakura, D. Ito, D. Ivankovic, S. Ivanova, A. K. V. Iyer, J. M. Izquierdo, M. Izumi, M. Jaattela, M. S. Jabir, W. T. Jackson, N. Jacobo-Herrera, A. C. Jacomin, E. Jacquin, P. Jadiya, H. Jaeschke, C. Jagannath, A. J. Jakobi, J. Jakobsson, B. Janji, P. Jansen-Durr, P. J. Jansson, J. Jantsch, S. Januszewski, A. Jassey, S. Jean, H. Jeltsch-David, P. Jendelova, A. Jenny, T. E. Jensen, N. Jessen, J. L. Jewell, J. Ji, L. Jia, R. Jia, L. Jiang, Q. Jiang, R. Jiang, T. Jiang, X. Jiang, Y. Jiang, M. Jimenez-Sanchez, E. J. Jin, F. Jin, H. Jin, L. Jin, L. Jin, M. Jin, S. Jin, E. K. Jo, C. Joffre, T. Johansen, G. V. W. Johnson, S. A. Johnston, E. Jokitalo, M. K. Jolly, L. A. B. Joosten, J. Jordan, B. Joseph, D. Ju, J. S. Ju, J. Ju, E. Juarez, D. Judith, G. Juhasz, Y. Jun, C. H. Jung, S. C. Jung, Y. K. Jung, H. Jungbluth, J. Jungverdorben, S. Just, K. Kaarniranta, A. Kaasik, T. Kabuta, D. Kaganovich, A. Kahana, R. Kain, S. Kajimura, M. Kalamvoki, M. Kalia, D. S. Kalinowski, N. Kaludercic, I. Kalvari, J. Kaminska, V. O. Kaminskyy, H. Kanamori, K. Kanasaki, C. Kang, R. Kang, S. S. Kang, S. Kaniyappan, T. Kanki, T. D. Kanneganti, A. G. Kanthasamy, A. Kanthasamy, M. Kantorow, O. Kapuy, M. V. Karamouzis, M. R. Karim, P. Karmakar, R. G. Katare, M. Kato, S. H. E. Kaufmann, A. Kauppinen, G. P. Kaushal, S. Kaushik, K. Kawasaki, K. Kazan, P. Y. Ke, D. J. Keating, U. Keber, J. H. Kehrl, K. E. Keller, C. W. Keller, J. K. Kemper, C. M. Kenific, O. Kepp, S. Kermorgant, A. Kern, R. Ketteler, T. G. Keulers, B. Khalfin, H. Khalil, B. Khambu, S. Y. Khan, V. K. M. Khandelwal, R. Khandia, W. Kho, N. V. Khobrekar, S. Khuansuwan, M. Khundadze, S. A. Killackey, D. Kim, D. R. Kim, D. H. Kim, D. E. Kim, E. Y. Kim, E. K. Kim, H. R. Kim, H. S. Kim, K. Hyung-Ryong, J. H. Kim, J. K. Kim, J. H. Kim, J. H. Kim, K. I. Kim, P. K. Kim, S. J. Kim, S. R. Kimball, A. Kimchi, A. C. Kimmelman, T. Kimura, M. A. King, K. J. Kinghorn, C. G. Kinsey, V. Kirkin, L. A. Kirshenbaum, S. L. Kiselev, S. Kishi, K. Kitamoto, Y. Kitaoka, K. Kitazato, R. N. Kitsis, J. T. Kittler, O. Kjaerulff, P. S. Klein, T. Klopstock, J. Klucken, H. Knaevelsrud, R. L. Knorr, B. C. B. Ko, F. Ko, J. L. Ko, H. Kobayashi, S. Kobayashi, I. Koch, J. C. Koch, U. Koenig, D. Kogel, Y. H. Koh, M. Koike, S. D. Kohlwein, N. M. Kocaturk, M. Komatsu, J. Konig, T. Kono, B. T. Kopp, T. Korcsmaros, G. Korkmaz, V. I. Korolchuk, M. S. Korsnes, A. Koskela, J. Kota, Y. Kotake, M. L. Kotler, Y. Kou, M. I. Koukourakis, E. Koustas, A. L. Kovacs, T. Kovacs, D. Koya, T. Kozako, C. Kraft, D. Krainc, H. Kramer, A. D. Krasnodembskaya, C. Kretz-Remy, G. Kroemer, N. T. Ktistakis, K. Kuchitsu, S. Kuenen, L. Kuerschner, T. Kukar, A. Kumar, A. Kumar, D. Kumar, D. Kumar, S. Kumar, S. Kume, C. Kumsta, C. N. Kundu, M. Kundu, A. B. Kunnumakkara, L. Kurgan, T. G. Kutateladze, O. Kutlu, S. Kwak, H. J. Kwon, T. K. Kwon, Y. T. Kwon, I. Kyrmizi, A. La Spada, P. Labonte, S. Ladoire, I. Laface, F. Lafont, D. C. Lagace, V. Lahiri, Z. Lai, A. S. Laird, A. Lakkaraju, T. Lamark, S. H. Lan, A. Landajuela, D. J. R. Lane, J. D. Lane, C. H. Lang, C. Lange, U. Langel, R. Langer, P. Lapaquette, J. Laporte, N. F. LaRusso, I. Lastres-Becker, W. C. Y. Lau, G. W. Laurie, S. Lavandero, B. Y. K. Law, H. K. Law, R. Layfield, W. Le, H. Le Stunff, A. Y. Leary, J. J. Lebrun, L. Y. W. Leck, J. P. Leduc-Gaudet, C. Lee, C. P. Lee, D. H. Lee, E. B. Lee, E. F. Lee, G. M. Lee, H. J. Lee, H. K. Lee, J. M. Lee, J. S. Lee, J. A. Lee, J. Y. Lee, J. H. Lee, M. Lee, M. G. Lee, M. J. Lee, M. S. Lee, S. Y. Lee, S. J. Lee, S. Y. Lee, S. B. Lee, W. H. Lee, Y. R. Lee, Y. H. Lee, Y. Lee, C. Lefebvre, R. Legouis, Y. L. Lei, Y. Lei, S. Leikin, G. Leitinger, L. Lemus, S. Leng, O. Lenoir, G. Lenz, H. J. Lenz, P. Lenzi, Y. Leon, A. M. Leopoldino, C. Leschczyk, S. Leskela, E. Letellier, C. T. Leung, P. S. Leung, J. S. Leventhal, B. Levine, P. A. Lewis, K. Ley, B. Li, D. Q. Li, J. Li, J. Li, J. Li, K. Li, L. Li, M. Li, M. Li, M. Li, M. Li, M. Li, P. L. Li, M. Q. Li, Q. Li, S. Li, T. Li, W. Li, W. Li, X. Li, Y. P. Li, Y. Li, Z. Li, Z. Li, Z. Li, J. Lian, C. Liang, Q. Liang, W. Liang, Y. Liang, Y. Liang, G. Liao, L. Liao, M. Liao, Y. F. Liao, M. Librizzi, P. P. Y. Lie, M. A. Lilly, H. J. Lim, T. R. R. Lima, F. Limana, C. Lin, C. W. Lin, D. S. Lin, F. C. Lin, J. D. Lin, K. M. Lin, K. H. Lin, L. T. Lin, P. H. Lin, Q. Lin, S. Lin, S. J. Lin, W. Lin, X. Lin, Y. X. Lin, Y. S. Lin, R. Linden, P. Lindner, S. C. Ling, P. Lingor, A. K. Linnemann, Y. C. Liou, M. M. Lipinski, S. Lipovsek, V. A. Lira, N. Lisiak, P. B. Liton, C. Liu, C. H. Liu, C. F. Liu, C. H. Liu, F. Liu, H. Liu, H. S. Liu, H. F. Liu, H. Liu, J. Liu, J. Liu, J. Liu, L. Liu, L. Liu, M. Liu, Q. Liu, W. Liu, W. Liu, X. H. Liu, X. Liu, X. Liu, X. Liu, X. Liu, Y. Liu, Y. Liu, Y. Liu, Y. Liu, Y. Liu, J. A. Livingston, G. Lizard, J. M. Lizcano, S. Ljubojevic-Holzer, L. L. ME, D. Llobet-Navas, A. Llorente, C. H. Lo, D. Lobato-Marquez, Q. Long, Y. C. Long, B. Loos, J. A. Loos, M. G. Lopez, G. Lopez-Domenech, J. A. Lopez-Guerrero, A. T. Lopez-Jimenez, O. Lopez-Perez, I. Lopez-Valero, M. J. Lorenowicz, M. Lorente, P. Lorincz, L. Lossi, S. Lotersztajn, P. E. Lovat, J. F. Lovell, A. Lovy, P. Low, G. Lu, H. Lu, J. H. Lu, J. J. Lu, M. Lu, S. Lu, A. Luciani, J. M. Lucocq, P. Ludovico, M. A. Luftig, M. Luhr, D. Luis-Ravelo, J. J. Lum, L. Luna-Dulcey, A. H. Lund, V. K. Lund, J. D. Lunemann, P. Luningschror, H. Luo, R. Luo, S. Luo, Z. Luo, C. Luparello, B. Luscher, L. Luu, A. Lyakhovich, K. G. Lyamzaev, A. H. Lystad, L. Lytvynchuk, A. C. Ma, C. Ma, M. Ma, N. F. Ma, Q. H. Ma, X. Ma, Y. Ma, Z. Ma, O. A. MacDougald, F. Macian, G. C. MacIntosh, J. P. MacKeigan, K. F. Macleod, S. Maday, F. Madeo, M. Madesh, T. Madl, J. Madrigal-Matute, A. Maeda, Y. Maejima, M. Magarinos, P. Mahavadi, E. Maiani, K. Maiese, P. Maiti, M. C. Maiuri, B. Majello, M. B. Major, E. Makareeva, F. Malik, K. Mallilankaraman, W. Malorni, A. Maloyan, N. Mammadova, G. C. W. Man, F. Manai, J. D. Mancias, E. M. Mandelkow, M. A. Mandell, A. A. Manfredi, M. H. Manjili, R. Manjithaya, P. Manque, B. B. Manshian, R. Manzano, C. Manzoni, K. Mao, C. Marchese, S. Marchetti, A. M. Marconi, F. Marcucci, S. Mardente, O. A. Mareninova, M. Margeta, M. Mari, S. Marinelli, O. Marinelli, G. Marino, S. Mariotto, R. S. Marshall, M. R. Marten, S. Martens, A. P. J. Martin, K. R. Martin, S. Martin, S. Martin, A. Martin-Segura, M. A. Martin-Acebes, I. Martin-Burriel, M. Martin-Rincon, P. Martin-Sanz, J. A. Martina, W. Martinet, A. Martinez, A. Martinez, J. Martinez, M. M. Velazquez, N. Martinez-Lopez, M. Martinez-Vicente, D. O. Martins, J. O. Martins, W. K. Martins, T. Martins-Marques, E. Marzetti, S. Masaldan, C. Masclaux-Daubresse, D. G. Mashek, V. Massa, L. Massieu, G. R. Masson, L. Masuelli, A. I. Masyuk, T. V. Masyuk, P. Matarrese, A. Matheu, S. Matoba, S. Matsuzaki, P. Mattar, A. Matte, D. Mattoscio, J. L. Mauriz, M. Mauthe, C. Mauvezin, E. Maverakis, P. Maycotte, J. Mayer, G. Mazzoccoli, C. Mazzoni, J. R. Mazzulli, N. McCarty, C. McDonald, M. R. McGill, S. L. McKenna, B. McLaughlin, F. McLoughlin, M. A. McNiven, T. G. McWilliams, F. Mechta-Grigoriou, T. C. Medeiros, D. L. Medina, L. A. Megeney, K. Megyeri, M. Mehrpour, J. L. Mehta, A. J. Meijer, A. H. Meijer, J. Mejlvang, A. Melendez, A. Melk, G. Memisoglu, A. F. Mendes, D. Meng, F. Meng, T. Meng, R. Menna-Barreto, M. B. Menon, C. Mercer, A. E. Mercier, J. L. Mergny, A. Merighi, S. D. Merkley, G. Merla, V. Meske, A. C. Mestre, S. P. Metur, C. Meyer, H. Meyer, W. Mi, J. Mialet-Perez, J. Miao, L. Micale, Y. Miki, E. Milan, M. Milczarek, D. L. Miller, S. I. Miller, S. Miller, S. W. Millward, I. Milosevic, E. A. Minina, H. Mirzaei, H. R. Mirzaei, M. Mirzaei, A. Mishra, N. Mishra, P. K. Mishra, M. M. Marjanovic, R. Misasi, A. Misra, G. Misso, C. Mitchell, G. Mitou, T. Miura, S. Miyamoto, M. Miyazaki, M. Miyazaki, T. Miyazaki, K. Miyazawa, N. Mizushima, T. H. Mogensen, B. Mograbi, R. Mohammadinejad, Y. Mohamud, A. Mohanty, S. Mohapatra, T. Mohlmann, A. Mohmmed, A. Moles, K. H. Moley, M. Molinari, V. Mollace, A. B. Moller, B. Mollereau, F. Mollinedo, C. Montagna, M. J. Monteiro, A. Montella, L. R. Montes, B. Montico, V. K. Mony, G. M. Compagnoni, M. N. Moore, M. A. Moosavi, A. L. Mora, M. Mora, D. Morales-Alamo, R. Moratalla, P. I. Moreira, E. Morelli, S. Moreno, D. Moreno-Blas, V. Moresi, B. Morga, A. H. Morgan, F. Morin, H. Morishita, O. L. Moritz, M. Moriyama, Y. Moriyasu, M. Morleo, E. Morselli, J. F. Moruno-Manchon, J. Moscat, S. Mostowy, E. Motori, A. F. Moura, N. Moustaid-Moussa, M. Mrakovcic, G. Mucino-Hernandez, A. Mukherjee, S. Mukhopadhyay, J. M. M. Levy, V. Mulero, S. Muller, C. Munch, A. Munjal, P. Munoz-Canoves, T. Munoz-Galdeano, C. Munz, T. Murakawa, C. Muratori, B. M. Murphy, J. P. Murphy, A. Murthy, T. T. Myohanen, I. U. Mysorekar, J. Mytych, S. M. Nabavi, M. Nabissi, P. Nagy, J. Nah, A. Nahimana, I. Nakagawa, K. Nakamura, H. Nakatogawa, S. S. Nandi, M. Nanjundan, M. Nanni, G. Napolitano, R. Nardacci, M. Narita, M. Nassif, I. Nathan, M. Natsumeda, R. J. Naude, C. Naumann, O. Naveiras, F. Navid, S. T. Nawrocki, T. Y. Nazarko, F. Nazio, F. Negoita, T. Neill, A. L. Neisch, L. M. Neri, M. G. Netea, P. Neubert, T. P. Neufeld, D. Neumann, A. Neutzner, P. T. Newton, P. A. Ney, I. P. Nezis, C. C. W. Ng, T. B. Ng, H. T. T. Nguyen, L. T. Nguyen, H. M. Ni, C. N. Cheallaigh, Z. Ni, M. C. Nicolao, F. Nicoli, M. Nieto-Diaz, P. Nilsson, S. Ning, R. Niranjan, H. Nishimune, M. Niso-Santano, R. A. Nixon, A. Nobili, C. Nobrega, T. Noda, U. Nogueira-Recalde, T. M. Nolan, I. Nombela, I. Novak, B. Novoa, T. Nozawa, N. Nukina, C. Nussbaum-Krammer, J. Nylandsted, T. R. O'Donovan, S. M. O'Leary, E. J. O'Rourke, M. P. O'Sullivan, T. E. O'Sullivan, S. Oddo, I. Oehme, M. Ogawa, E. Ogier-Denis, M. H. Ogmundsdottir, B. Ogretmen, G. T. Oh, S. H. Oh, Y. J. Oh, T. Ohama, Y. Ohashi, M. Ohmuraya, V. Oikonomou, R. Ojha, K. Okamoto, H. Okazawa, M. Oku, S. Olivan, J. M. A. Oliveira, M. Ollmann, J. A. Olzmann, S. Omari, M. B. Omary, G. Onal, M. Ondrej, S. B. Ong, S. G. Ong, A. Onnis, J. A. Orellana, S. Orellana-Munoz, M. D. M. Ortega-Villaizan, X. R. Ortiz-Gonzalez, E. Ortona, H. D. Osiewacz, A. K. Osman, R. Osta, M. S. Otegui, K. Otsu, C. Ott, L. Ottobrini, J. J. Ou, T. F. Outeiro, I. Oynebraten, M. Ozturk, G. Pages, S. Pahari, M. Pajares, U. B. Pajvani, R. Pal, S. Paladino, N. Pallet, M. Palmieri, G. Palmisano, C. Palumbo, F. Pampaloni, L. Pan, Q. Pan, W. Pan, X. Pan, G. Panasyuk, R. Pandey, U. B. Pandey, V. Pandya, F. Paneni, S. Y. Pang, E. Panzarini, D. L. Papademetrio, E. Papaleo, D. Papinski, D. Papp, E. C. Park, H. T. Park, J. M. Park, J. I. Park, J. T. Park, J. Park, S. C. Park, S. Y. Park, A. H. Parola, J. B. Parys, A. Pasquier, B. Pasquier, J. F. Passos, N. Pastore, H. H. Patel, D. Patschan, S. Pattingre, G. Pedraza-Alva, J. Pedraza-Chaverri, Z. Pedrozo, G. Pei, J. Pei, H. Peled-Zehavi, J. M. Pellegrini, J. Pelletier, M. A. Penalva, D. Peng, Y. Peng, F. Penna, M. Pennuto, F. Pentimalli, C. M. Pereira, G. J. S. Pereira, L. C. Pereira, L. P. de Almeida, N. D. Perera, A. Perez-Lara, A. B. Perez-Oliva, M. E. Perez-Perez, P. Periyasamy, A. Perl, C. Perrotta, I. Perrotta, R. G. Pestell, M. Petersen, I. Petrache, G. Petrovski, T. Pfirrmann, A. S. Pfister, J. A. Philips, H. Pi, A. Picca, A. M. Pickrell, S. Picot, G. M. Pierantoni, M. Pierdominici, P. Pierre, V. Pierrefite-Carle, K. Pierzynowska, F. Pietrocola, M. Pietruczuk, C. Pignata, F. X. Pimentel-Muinos, M. Pinar, R. O. Pinheiro, R. Pinkas-Kramarski, P. Pinton, K. Pircs, S. Piya, P. Pizzo, T. S. Plantinga, H. W. Platta, A. Plaza-Zabala, M. Plomann, E. Y. Plotnikov, H. Plun-Favreau, R. Pluta, R. Pocock, S. Poggeler, C. Pohl, M. Poirot, A. Poletti, M. Ponpuak, H. Popelka, B. Popova, H. Porta, S. P. Alcon, E. Portilla-Fernandez, M. Post, M. B. Potts, J. Poulton, T. Powers, V. Prahlad, T. K. Prajsnar, D. Pratico, R. Prencipe, M. Priault, T. Proikas-Cezanne, V. J. Promponas, C. G. Proud, R. Puertollano, L. Puglielli, T. Pulinilkunnil, D. Puri, R. Puri, J. Puyal, X. Qi, Y. Qi, W. Qian, L. Qiang, Y. Qiu, J. Quadrilatero, J. Quarleri, N. Raben, H. Rabinowich, D. Ragona, M. J. Ragusa, N. Rahimi, M. Rahmati, V. Raia, N. Raimundo, N. S. Rajasekaran, S. R. Rao, A. Rami, I. Ramirez-Pardo, D. B. Ramsden, F. Randow, P. N. Rangarajan, D. Ranieri, H. Rao, L. Rao, R. Rao, S. Rathore, J. A. Ratnayaka, E. A. Ratovitski, P. Ravanan, G. Ravegnini, S. K. Ray, B. Razani, V. Rebecca, F. Reggiori, A. Regnier-Vigouroux, A. S. Reichert, D. Reigada, J. H. Reiling, T. Rein, S. Reipert, R. S. Rekha, H. Ren, J. Ren, W. Ren, T. Renault, G. Renga, K. Reue, K. Rewitz, B. R. de Andrade Ramos, S. A. Riazuddin, T. M. Ribeiro-Rodrigues, J. E. Ricci, R. Ricci, V. Riccio, D. R. Richardson, Y. Rikihisa, M. V. Risbud, R. M. Risueno, K. Ritis, S. Rizza, R. Rizzuto, H. C. Roberts, L. D. Roberts, K. J. Robinson, M. C. Roccheri, S. Rocchi, G. G. Rodney, T. Rodrigues, V. R. R. Silva, A. Rodriguez, R. Rodriguez-Barrueco, N. Rodriguez-Henche, H. Rodriguez-Rocha, J. Roelofs, R. S. Rogers, V. V. Rogov, A. I. Rojo, K. Rolka, V. Romanello, L. Romani, A. Romano, P. S. Romano, D. Romeo-Guitart, L. C. Romero, M. Romero, J. C. Roney, C. Rongo, S. Roperto, M. T. Rosenfeldt, P. Rosenstiel, A. G. Rosenwald, K. A. Roth, L. Roth, S. Roth, K. M. A. Rouschop, B. D. Roussel, S. Roux, P. Rovere-Querini, A. Roy, A. Rozieres, D. Ruano, D. C. Rubinsztein, M. P. Rubtsova, K. Ruckdeschel, C. Ruckenstuhl, E. Rudolf, R. Rudolf,

A. Ruggieri, A. A. Ruparelia, P. Rusmini, R. R. Russell, G. L. Russo, M. Russo, R. Russo, O. O. Ryabaya, K. M. Ryan, K. Y. Ryu, M. Sabater-Arcis, U. Sachdev, M. Sacher, C. Sachse, A. Sadhu, J. Sadoshima, N. Safren, P. Saftig, A. P. Sagona, G. Sahay, A. Sahebkar, M. Sahin, O. Sahin, S. Sahni, N. Saito, S. Saito, T. Saito, R. Sakai, Y. Sakai, J. I. Sakamaki, K. Saksela, G. Salazar, A. Salazar-Degracia, G. H. Salekdeh, A. K. Saluja, B. Sampaio-Marques, M. C. Sanchez, J. A. Sanchez-Alcazar, V. Sanchez-Vera, V. Sancho-Shimizu, J. T. Sanderson, M. Sandri, S. Santaguida, L. Santambrogio, M. M. Santana, G. Santoni, A. Sanz, P. Sanz, S. Saran, M. Sardiello, T. J. Sargeant, A. Sarin, C. Sarkar, S. Sarkar, M. R. Sarrias, S. Sarkar, D. T. Sarmah, J. Sarparanta, A. Sathyanarayan, R. Sathyanarayanan, K. M. Scaglione, F. Scatozza, L. Schaefer, Z. T. Schafer, U. E. Schaible, A. H. V. Schapira, M. Scharl, H. M. Schatzl, C. H. Schein, W. Scheper, D. Scheuring, M. V. Schiaffino, M. Schiappacassi, R. Schindl, U. Schlattner, O. Schmidt, R. Schmitt, S. D. Schmidt, I. Schmitz, E. Schmukler, A. Schneider, B. E. Schneider, R. Schober, A. C. Schoijet, M. B. Schott, M. Schramm, B. Schroder, K. Schuh, C. Schuller, R. J. Schulze, L. Schurmanns, J. C. Schwamborn, M. Schwarten, F. Scialo, S. Sciarretta, M. J. Scott, K. W. Scotto, A. I. Scovassi, A. Scrima, A. Scrivo, D. Sebastian, S. Sebti, S. Sedej, L. Segatori, N. Segev, P. O. Seglen, I. Seiliez, E. Seki, S. B. Selleck, F. W. Sellke, J. T. Selsby, M. Sendtner, S. Senturk, E. Seranova, C. Sergi, R. Serra-Moreno, H. Sesaki, C. Settembre, S. R. G. Setty, G. Sgarbi, O. Sha, J. J. Shacka, J. A. Shah, D. Shang, C. Shao, F. Shao, S. Sharbati, L. M. Sharkey, D. Sharma, G. Sharma, K. Sharma, P. Sharma, S. Sharma, H. M. Shen, H. Shen, J. Shen, M. Shen, W. Shen, Z. Shen, R. Sheng, Z. Sheng, Z. H. Sheng, J. Shi, X. Shi, Y. H. Shi, K. Shiba-Fukushima, J. J. Shieh, Y. Shimada, S. Shimizu, M. Shimozawa, T. Shintani, C. J. Shoemaker, S. Shojaei, I. Shoji, B. V. Shravage, V. Shridhar, C. W. Shu, H. B. Shu, K. Shui, A. K. Shukla, T. E. Shutt, V. Sica, A. Siddiqui, A. Sierra, V. Sierra-Torre, S. Signorelli, P. Sil, B. J. A. Silva, J. D. Silva, E. Silva-Pavez, S. Silvente-Poirot, R. E. Simmonds, A. K. Simon, H. U. Simon, M. Simons, A. Singh, L. P. Singh, R. Singh, S. V. Singh, S. K. Singh, S. B. Singh, S. Singh, S. P. Singh, D. Sinha, R. A. Sinha, S. Sinha, A. Sirko, K. Sirohi, E. L. Sivridis, P. Skendros, A. Skirycz, I. Slaninova, S. S. Smaili, A. Smertenko, M. D. Smith, S. J. Soenen, E. J. Sohn, S. P. M. Sok, G. Solaini, T. Soldati, S. A. Soleimanpour, R. M. Soler, A. Solovchenko, J. A. Somarelli, A. Sonawane, F. Song, H. K. Song, J. X. Song, K. Song, Z. Song, L. R. Soria, M. Sorice, A. A. Soukas, S. F. Soukup, D. Sousa, N. Sousa, P. A. Spagnuolo, S. A. Spector, M. M. S. Bharath, D. S. Clair, V. Stagni, L. Staiano, C. A. Stalnecker, M. V. Stankov, P. B. Stathopulos, K. Stefan, S. M. Stefan, L. Stefanis, J. S. Steffan, A. Steinkasserer, H. Stenmark, J. Sterneckert, C. Stevens, V. Stoka, S. Storch, B. Stork, F. Strappazzon, A. M. Strohecker, D. G. Stupack, H. Su, L. Y. Su, L. Su, A. M. Suarez-Fontes, C. S. Subauste, S. Subbian, P. V. Subirada, G. Sudhandiran, C. M. Sue, X. Sui, C. Summers, G. Sun, J. Sun, K. Sun, M. X. Sun, Q. Sun, Y. Sun, Z. Sun, K. K. S. Sunahara, E. Sundberg, K. Susztak, P. Sutovsky, H. Suzuki, G. Sweeney, J. D. Symons, S. C. W. Sze, N. J. Szewczyk, A. Tabecka-Lonczynska, C. Tabolacci, F. Tacke, H. Taegtmeyer, M. Tafani, M. Tagaya, H. Tai, S. W. G. Tait, Y. Takahashi, S. Takats, P. Talwar, C. Tam, S. Y. Tam, D. Tampellini, A. Tamura, C. T. Tan, E. K. Tan, Y. Q. Tan, M. Tanaka, M. Tanaka, D. Tang, J. Tang, T. S. Tang, I. Tanida, Z. Tao, M. Taouis, L. Tatenhorst, N. Tavernarakis, A. Taylor, G. A. Taylor, J. M. Taylor, E. Tchetina, A. R. Tee, I. Tegeder, D. Teis, N. Teixeira, F. Teixeira-Clerc, K. A. Tekirdag, T. Tencomnao, S. Tenreiro, A. V. Tepikin, P. S. Testillano, G. Tettamanti, P. L. Tharaux, K. Thedieck, A. A. Thekkinghat, S. Thellung, J. W. Thinwa, V. P. Thirumalaikumar, S. M. Thomas, P. G. Thomes, A. Thorburn, L. Thukral, T. Thum, M. Thumm, L. Tian, A. Tichy, A. Till, V. Timmerman, V. I. Titorenko, S. V. Todi, K. Todorova, J. M. Toivonen, L. Tomaipitinca, D. Tomar, C. Tomas-Zapico, S. Tomic, B. C. Tong, C. Tong, X. Tong, S. A. Tooze, M. L. Torgersen, S. Torii, L. Torres-Lopez, A. Torriglia, C. G. Towers, R. Towns, S. Toyokuni, V. Trajkovic, D. Tramontano, Q. G. Tran, L. H. Travassos, C. B. Trelford, S. Tremel, I. P. Trougakos, B. P. Tsao, M. P. Tschan, H. F. Tse, T. F. Tse, H. Tsugawa, A. S. Tsvetkov, D. A. Tumbarello, Y. Tumtas, M. J. Tunon, S. Turcotte, B. Turk, V. Turk, B. J. Turner, R. I. Tuxworth, J. K. Tyler, E. V. Tyutereva, Y. Uchiyama, A. Ugun-Klusek, H. H. Uhlig, M. Ulamek-Koziol, I. V. Ulasov, M. Umekawa, C. Ungermann, R. Unno, S. Urbe, E. Uribe-Carretero, S. Ustun, V. N. Uversky, T. Vaccari, M. I. Vaccaro, B. F. Vahsen, H. Vakifahmetoglu-Norberg, R. Valdor, M. J. Valente, A. Valko, R. B. Vallee, A. M. Valverde, G. Van den Berghe, S. van der Veen, L. Van Kaer, J. van Loosdregt, S. J. L. van Wijk, W. Vandenberghe, I. Vanhorebeek, M. A. Vannier-Santos, N. Vannini, M. C. Vanrell, C. Vantaggiato, G. Varano, I. Varela-Nieto, M. Varga, M. H. Vasconcelos, S. Vats, D. G. Vavvas, I. Vega-Naredo, S. Vega-Rubin-de-Celis, G. Velasco, A. P. Velazquez, T. Vellai, E. Vellenga, F. Velotti, M. Verdier, P. Verginis, I. Vergne, P. Verkade, M. Verma, P. Verstreken, T. Vervliet, J. Vervoorts, A. T. Vessoni, V. M. Victor, M. Vidal, C. Vidoni, O. V. Vieira, R. D. Vierstra, S. Vigano, H. Vihinen, V. Vijayan, M. Vila, M. Vilar, J. M. Villalba, A. Villalobo, B. Villarejo-Zori, F. Villarroya, J. Villarroya, O. Vincent, C. Vindis, C. Viret, M. T. Viscomi, D. Visnjic, I. Vitale, D. J. Vocadlo, O. V. Voitsekhovskaja, C. Volonte, M. Volta, M. Vomero, C. Von Haefen, M. A. Vooijs, W. Voos, L. Vucicevic, R. Wade-Martins, S. Waguri, K. A. Waite, S. Wakatsuki, D. W. Walker, M. J. Walker, S. A. Walker, J. Walter, F. G. Wandosell, B. Wang, C. Y. Wang, C. Wang, C. Wang, C. Wang, C. Y. Wang, D. Wang, F. Wang, F. Wang, F. Wang, G. Wang, H. Wang, H. Wang, H. Wang, H. G. Wang, J. Wang, J. Wang, J. Wang, J. Wang, K. Wang, L. Wang, L. Wang, M. H. Wang, M. Wang, N. Wang, P. Wang, P. Wang, Q. J. Wang, Q. Wang, Q. K. Wang, Q. A. Wang, W. T. Wang, W. Wang, X. Wang, X. Wang, Y. Wang, Y. Wang, Y. Y. Wang, Y. Wang, Y. Wang, Y. Wang, Y. Wang, Z. Wang, Z. Wang, G. Warnes, V. Warnsmann, H. Watada, E. Watanabe, M. Watchon, A. Wawrzynska, T. E. Weaver, G. Wegrzyn, A. M. Wehman, H. Wei, L. Wei, T. Wei, Y. Wei, O. H. Weiergraber, C. C. Weihl, G. Weindl, R. Weiskirchen, A. Wells, R. H. Wen, X. Wen, A. Werner, B. Weykopf, S. P. Wheatley, J. L. Whitton, A. J. Whitworth, K. Wiktorska, M. E. Wildenberg, T. Wileman, S. Wilkinson, D. Willbold, B. Williams, R. S. B. Williams, R. L. Williams, P. R. Williamson, R. A. Wilson, B. Winner, N. J. Winsor, S. S. Witkin, H. Wodrich, U. Woehlbier, T. Wollert, E. Wong, J. H. Wong, R. W. Wong, V. K. W. Wong, W. W. Wong, A. G. Wu, C. Wu, J. Wu, J. Wu, K. K. Wu, M. Wu, S. Y. Wu, S. Wu, S. Y. Wu, S. Wu, W. K. K. Wu, X. Wu, X. Wu, Y. W. Wu, Y. Wu, R. J. Xavier, H. Xia, L. Xia, Z. Xia, G. Xiang, J. Xiang, M. Xiang, W. Xiang, B. Xiao, G. Xiao, H. Xiao, H. T. Xiao, J. Xiao, L. Xiao, S. Xiao, Y. Xiao, B. Xie, C. M. Xie, M. Xie, Y. Xie, Z. Xie, Z. Xie, M. Xilouri, C. Xu, E. Xu, H. Xu, J. Xu, J. Xu, L. Xu, W. W. Xu, X. Xu, Y. Xue, S. M. S. Yakhine-Diop, M. Yamaguchi, O. Yamaguchi, A. Yamamoto, S. Yamashina, S. Yan, S. J. Yan, Z. Yan, Y. Yanagi, C. Yang, D. S. Yang, H. Yang, H. T. Yang, H. Yang, J. M. Yang, J. Yang, J. Yang, L. Yang, L. Yang, M. Yang, P. M. Yang, Q. Yang, S. Yang, S. Yang, F. Yang, W. Yang, W. Y. Yang, X. Yang, X. Yang, Y. Yang, H. Yao, S. Yao, X. Yao, Y. G. Yao, Y. M. Yao, T. Yasui, M. Yazdankhah, P. M. Yen, C. Yi, X. M. Yin, Y. Yin, Z. Yin, Z. Yin, M. Ying, Z. Ying, C. K. Yip, S. P. T. Yiu, Y. H. Yoo, K. Yoshida, S. R. Yoshii, T. Yoshimori, B. Yousefi, B. Yu, H. Yu, J. Yu, J. Yu, L. Yu, M. L. Yu, S. W. Yu, V. C. Yu, W. H. Yu, Z. Yu, Z. Yu, J. Yuan, L. Q. Yuan, S. Yuan, S. F. Yuan, Y. Yuan, Z. Yuan, J. Yue, Z. Yue, J. Yun, R. L. Yung, D. N. Zacks, G. Zaffagnini, V. O. Zambelli, I. Zanella, Q. S. Zang, S. Zanivan, S. Zappavigna, P. Zaragoza, K. S. Zarbalis, A. Zarebkohan, A. Zarrouk, S. O. Zeitlin, J. Zeng, J. D. Zeng, E. Zerovnik, L. Zhan, B. Zhang, D. D. Zhang, H. Zhang, H. Zhang, H. Zhang, H. Zhang, H. Zhang, H. Zhang, H. L. Zhang, J. Zhang, J. Zhang, J. P. Zhang, K. Y. B. Zhang, L. W. Zhang, L. Zhang, L. Zhang, L. Zhang, L. Zhang, M. Zhang, P. Zhang, S. Zhang, W. Zhang, X. Zhang, X. W. Zhang, X. Zhang, X. Zhang, X. Zhang, X. Zhang, X. D. Zhang, Y. Zhang, Y. Zhang, Y. Zhang, Y. D. Zhang, Y. Zhang, Y. Y. Zhang, Y. Zhang, Z. Zhang, Z. Zhang, Z. Zhang, Z. Zhang, Z. Zhang, H. Zhao, L. Zhao, S. Zhao, T. Zhao, X. F. Zhao, Y. Zhao, Y. Zhao, Y. Zhao, Y. Zhao, G. Zheng, K. Zheng, L. Zheng, S. Zheng, X. L. Zheng, Y. Zheng, Z. G. Zheng, B. Zhivotovsky, Q. Zhong, A. Zhou, B. Zhou, C. Zhou, G. Zhou, H. Zhou, H. Zhou, H. Zhou, J. Zhou, J. Zhou, J. Zhou, J. Zhou, K. Zhou, R. Zhou, X. J. Zhou, Y. Zhou, Y. Zhou, Y. Zhou, Z. Y. Zhou, Z. Zhou, B. Zhu, C. Zhu, G. Q. Zhu, H. Zhu, H. Zhu, H. Zhu, W. G. Zhu, Y. Zhu, Y. Zhu, H. Zhuang, X. Zhuang, K. Zientara-Rytter, C. M. Zimmermann, E. Ziviani, T. Zoladek, W. X. Zong, D. B. Zorov, A. Zorzano, W. Zou, Z. Zou, Z. Zou, S. Zuryn, W. Zwerschke, B. Brand-Saberi, X. C. Dong, C. S. Kenchappa, Z. Li, Y. Lin, S. Oshima, Y. Rong, J. C. Sluimer, C. L. Stallings, C. K. Tong, Guidelines for the use and interpretation of assays for monitoring autophagy (4th edition)[1]. *Autophagy* **17**, 1–382 (2021).

39. N. Yuan, L. Song, S. Zhang, W. Lin, Y. Cao, F. Xu, Y. Fang, Z. Wang, H. Zhang, X. Li, Z. Wang, J. Cai, J. Wang, Y. Zhang, X. Mao, W. Zhao, S. Hu, S. Chen, J. Wang, Bafilomycin A1 targets both autophagy and apoptosis pathways in pediatric B-cell acute lymphoblastic leukemia. *Haematologica* **100**, 345–356 (2015).
40. Kaser, M. Kambacheld, B. Kisters-Woike, T. Langer, Oma1, a novel membrane-bound metallopeptidase in mitochondria with activities overlapping with the m-AAA protease. *J. Biol. Chem.* **278**, 46414–46423 (2003).
41. S. C. Leary, P. A. Cobine, T. Nishimura, R. M. Verdijk, R. de Krijger, R. de Coo, M. A. Tarnopolsky, D. R. Winge, E. A. Shoubridge, COX19 mediates the transduction of a mitochondrial redox signal from SCO1 that regulates ATP7A-mediated cellular copper efflux. *Mol. Biol. Cell* **24**, 683–691 (2013).
42. I. Bourges, C. Ramus, B. Mousson de Camaret, R. Beugnot, C. Remacle, P. Cardol, G. Hofhaus, J. P. Issartel, Structural organization of mitochondrial human complex I: Role of the ND4 and ND5 mitochondria-encoded subunits and interaction with prohibitin. *Biochem. J.* **383**, 491–499 (2004).
43. V. G. Zaha, L. H. Young, AMP-activated protein kinase regulation and biological actions in the heart. *Circ. Res.* **111**, 800–814 (2012).
44. E. H. Ma, M. C. Poffenberger, A. H. Wong, R. G. Jones, The role of AMPK in T cell metabolism and function. *Curr. Opin. Immunol.* **46**, 45–52 (2017).
45. X. Liu, R. R. Chhipa, I. Nakano, B. Dasgupta, The AMPK inhibitor compound C is a potent AMPK-independent antiglioma agent. *Mol. Cancer Ther.* **13**, 596–605 (2014).
46. H. Zhu, Z. Liu, J. An, M. Zhang, Y. Qiu, M. H. Zou, Activation of AMPKα1 is essential for regulatory T cell function and autoimmune liver disease prevention. *Cell. Mol. Immunol.* **18**, 2609–2617 (2021).
47. A. P. Seabright, N. H. F. Fine, J. P. Barlow, S. O. Lord, I. Musa, A. Gray, J. A. Bryant, M. Banzhaf, G. G. Lavery, D. G. Hardie, D. J. Hodson, A. Philp, Y. C. Lai, AMPK activation induces mitophagy and promotes mitochondrial fission while activating TBK1 in a PINK1-Parkin independent manner. *FASEB J.* **34**, 6284–6301 (2020).
48. R. C. Laker, J. C. Drake, R. J. Wilson, V. A. Lira, B. M. Lewellen, K. A. Ryall, C. C. Fisher, M. Zhang, J. J. Saucerman, L. J. Goodyear, M. Kundu, Z. Yan, Ampk phosphorylation of Ulk1 is required for targeting of mitochondria to lysosomes in exercise-induced mitophagy. *Nat. Commun.* **8**, 548 (2017).
49. W. Tian, W. Li, Y. Chen, Z. Yan, X. Huang, H. Zhuang, W. Zhong, Y. Chen, W. Wu, C. Lin, H. Chen, X. Hou, L. Zhang, S. Sui, B. Zhao, Z. Hu, L. Li, D. Feng, Phosphorylation of ULK1 by

AMPK regulates translocation of ULK1 to mitochondria and mitophagy. *FEBS Lett.* **589**, 1847–1854 (2015).
50. S. Agarwal, C. M. Bell, S. B. Rothbart, R. G. Moran, AMP-activated protein kinase (AMPK) control of mTORC1 is p53- and TSC2-independent in Pemetrexed-treated carcinoma cells. *J. Biol. Chem.* **290**, 27473–27486 (2015).
51. S. Alers, A. S. Loffler, S. Wesselborg, B. Stork, Role of AMPK-mTOR-Ulk1/2 in the regulation of autophagy: Cross talk, shortcuts, and feedbacks. *Mol. Cell. Biol.* **32**, 2–11 (2012).
52. L. P. Poole, A. Bock-Hughes, D. E. Berardi, K. F. Macleod, ULK1 promotes mitophagy via phosphorylation and stabilization of BNIP3. *Sci. Rep.* **11**, 20526 (2021).
53. R. Q. Yao, C. Ren, Z. F. Xia, Y. M. Yao, Organelle-specific autophagy in inflammatory diseases: A potential therapeutic target underlying the quality control of multiple organelles. *Autophagy* **17**, 385–401 (2021).
54. S. Cipolat, O. Martins de Brito, B. Dal Zilio, L. Scorrano, OPA1 requires mitofusin 1 to promote mitochondrial fusion. *Proc. Natl. Acad. Sci. U.S.A.* **101**, 15927–15932 (2004).
55. A. Sood, D. V. Jeyaraju, J. Prudent, A. Caron, P. Lemieux, H. M. McBride, M. Laplante, K. Toth, L. Pellegrini, A Mitofusin-2-dependent inactivating cleavage of Opa1 links changes in mitochondria cristae and ER contacts in the postprandial liver. *Proc. Natl. Acad. Sci. U.S.A.* **111**, 16017–16022 (2014).
56. A. G. Gomez-Valades, M. Pozo, L. Varela, M. B. Boudjadja, S. Ramirez, I. Chivite, E. Eyre, R. Haddad-Tovolli, A. Obri, M. Mila-Guasch, J. Altirriba, M. Schneeberger, M. Imbernon, A. R. Garcia-Rendueles, P. Gama-Perez, J. Rojo-Ruiz, B. Racz, M. T. Alonso, R. Gomis, A. Zorzano, G. D'Agostino, C. V. Alvarez, R. Nogueiras, P. M. Garcia-Roves, T. L. Horvath, M. Claret, Mitochondrial cristae-remodeling protein OPA1 in POMC neurons couples Ca^{2+} homeostasis with adipose tissue lipolysis. *Cell Metab.* **33**, 1820–1835.e9 (2021).
57. T. E. O'Sullivan, L. R. Johnson, H. H. Kang, J. C. Sun, BNIP3- and BNIP3L-mediated mitophagy promotes the generation of natural killer cell memory. *Immunity* **43**, 331–342 (2015).
58. M. Z. Springer, L. P. Poole, L. E. Drake, A. Bock-Hughes, M. L. Boland, A. G. Smith, J. Hart, A. H. Chourasia, I. Liu, G. Bozek, K. F. Macleod, BNIP3-dependent mitophagy promotes cytosolic localization of LC3B and metabolic homeostasis in the liver. *Autophagy* **17**, 3530–3546 (2021).
59. K. Liu, Q. Zhao, H. Sun, L. Liu, C. Wang, Z. Li, Y. Xu, L. Wang, L. Zhang, H. Zhang, Q. Chen, T. Zhao, BNIP3 (BCL2 interacting protein 3) regulates pluripotency by modulating mitochondrial homeostasis via mitophagy. *Cell Death Dis.* **13**, 334 (2022).
60. A. Hurtado, K. A. Holmes, C. S. Ross-Innes, D. Schmidt, J. S. Carroll, FOXA1 is a key determinant of estrogen receptor function and endocrine response. *Nat. Genet.* **43**, 27–33 (2011).
61. K. H. Kaestner, The FoxA factors in organogenesis and differentiation. *Curr. Opin. Genet. Dev.* **20**, 527–532 (2010).
62. J. Laganiere, G. Deblois, C. Lefebvre, A. R. Bataille, F. Robert, V. Giguere, From the cover: Location analysis of estrogen receptor alpha target promoters reveals that FOXA1 defines a domain of the estrogen response. *Proc. Natl. Acad. Sci. U.S.A.* **102**, 11651–11656 (2005).
63. Z. Li, P. White, G. Tuteja, N. Rubins, S. Sackett, K. H. Kaestner, Foxa1 and Foxa2 regulate bile duct development in mice. *J. Clin. Invest.* **119**, 1537–1545 (2009).
64. M. Motallebipour, A. Ameur, M. S. Reddy Bysani, K. Patra, O. Wallerman, J. Mangion, M. A. Barker, K. J. McKernan, J. Komorowski, C. Wadelius, Differential binding and co-binding pattern of FOXA1 and FOXA3 and their relation to H3K4me3 in HepG2 cells revealed by ChIP-seq. *Genome Biol.* **10**, R129 (2009).
65. J. H. Taube, K. Allton, S. A. Duncan, L. Shen, M. C. Barton, Foxa1 functions as a pioneer transcription factor at transposable elements to activate Afp during differentiation of embryonic stem cells. *J. Biol. Chem.* **285**, 16135–16144 (2010).
66. N. Gao, J. Le Lay, W. Qin, N. Doliba, J. Schug, A. J. Fox, O. Smirnova, F. M. Matschinsky, K. H. Kaestner, Foxa1 and Foxa2 maintain the metabolic and secretory features of the mature beta-cell. *Mol. Endocrinol.* **24**, 1594–1604 (2010).
67. H. Y. Yim, Y. Yang, J. S. Lim, M. S. Lee, D. E. Zhang, K. I. Kim, The mitochondrial pathway and reactive oxygen species are critical contributors to interferon-α/β-mediated apoptosis in Ubp43-deficient hematopoietic cells. *Biochem. Biophys. Res. Commun.* **423**, 436–440 (2012).
68. J. A. Shyer, R. A. Flavell, W. Bailis, Author correction: Metabolic signaling in T cells. *Cell Res.* **30**, 1053 (2020).
69. L. Almeida, M. Lochner, L. Berod, T. Sparwasser, Metabolic pathways in T cell activation and lineage differentiation. *Semin. Immunol.* **28**, 514–524 (2016).
70. Y. Liu, I. Teige, B. Birnir, S. Issazadeh-Navikas, Neuron-mediated generation of regulatory T cells from encephalitogenic T cells suppresses EAE. *Nat. Med.* **12**, 518–525 (2006).
71. K. A. Mayer, U. Smole, C. Zhu, S. Derdak, A. A. Minervina, M. Salnikova, N. Witzeneder, A. Christamentl, N. Boucheron, P. Waidhofer-Sollner, M. Trauner, G. Hoermann, K. G. Schmetterer, I. Z. Mamedov, M. Bilban, W. Ellmeier, W. F. Pickl, G. A. Gualdoni, G. J. Zlabinger, The energy sensor AMPK orchestrates metabolic and translational adaptation in expanding T helper cells. *FASEB J.* **35**, e21217 (2021).
72. J. An, Y. Ding, C. Yu, J. Li, S. You, Z. Liu, P. Song, M. H. Zou, AMP-activated protein kinase alpha1 promotes tumor development via FOXP3 elevation in tumor-infiltrating Treg cells. *iScience* **25**, 103570 (2022).
73. A. M. J. Sanchez, R. Candau, H. Bernardi, AMP-activated protein kinase stabilizes FOXO3 in primary myotubes. *Biochem. Biophys. Res. Commun.* **499**, 493–498 (2018).
74. M. Matzinger, K. Fischhuber, D. Poloske, K. Mechtler, E. H. Heiss, AMPK leads to phosphorylation of the transcription factor Nrf2, tuning transactivation of selected target genes. *Redox Biol.* **29**, 101393 (2020).
75. M. Lippai, G. Csikos, P. Maroy, T. Lukacsovich, G. Juhasz, M. Sass, SNF4Agamma, the Drosophila AMPK gamma subunit is required for regulation of developmental and stress-induced autophagy. *Autophagy* **4**, 476–486 (2008).
76. P. Bharadwaj, R. N. Martins, PRKAG2 gene expression is elevated and its protein levels are associated with increased amyloid-β accumulation in the Alzheimer's disease brain. *J. Alzheimers Dis.* **74**, 441–448 (2020).
77. M. Palmieri, S. Impey, H. Kang, A. di Ronza, C. Pelz, M. Sardiello, A. Ballabio, Characterization of the CLEAR network reveals an integrated control of cellular clearance pathways. *Hum. Mol. Genet.* **20**, 3852–3866 (2011).
78. R. A. Hanna, M. N. Quinsay, A. M. Orogo, K. Giang, S. Rikka, A. B. Gustafsson, Microtubule-associated protein 1 light chain 3 (LC3) interacts with Bnip3 protein to selectively remove endoplasmic reticulum and mitochondria via autophagy. *J. Biol. Chem.* **287**, 19094–19104 (2012).
79. I. Novak, V. Kirkin, D. G. McEwan, J. Zhang, P. Wild, A. Rozenknop, V. Rogov, F. Lohr, D. Popovic, A. Occhipinti, A. S. Reichert, J. Terzic, V. Dotsch, P. A. Ney, I. Dikic, Nix is a selective autophagy receptor for mitochondrial clearance. *EMBO Rep.* **11**, 45–51 (2010).
80. Y. Zhu, S. Massen, M. Terenzio, V. Lang, S. Chen-Lindner, R. Eils, I. Novak, I. Dikic, A. Hamacher-Brady, N. R. Brady, Modulation of serines 17 and 24 in the LC3-interacting region of Bnip3 determines pro-survival mitophagy versus apoptosis. *J. Biol. Chem.* **288**, 1099–1113 (2013).
81. N. Gao, J. LeLay, M. Z. Vatamaniuk, S. Rieck, J. R. Friedman, K. H. Kaestner, Dynamic regulation of Pdx1 enhancers by Foxa1 and Foxa2 is essential for pancreas development. *Genes Dev.* **22**, 3435–3448 (2008).
82. S. Bittner, A. M. Afzali, H. Wiendl, S. G. Meuth, Myelin oligodendrocyte glycoprotein (MOG35-55) induced experimental autoimmune encephalomyelitis (EAE) in C57BL/6 mice. *J. Vis. Exp.* , 51275 (2014).
83. K. M. Curtis, L. A. Gomez, C. Rios, E. Garbayo, A. P. Raval, M. A. Perez-Pinzon, P. C. Schiller, EF1α and RPL13a represent normalization genes suitable for RT-qPCR analysis of bone marrow derived mesenchymal stem cells. *BMC Mol. Biol.* **11**, 61 (2010).
84. J. Schindelin, I. Arganda-Carreras, E. Frise, V. Kaynig, M. Longair, T. Pietzsch, S. Preibisch, C. Rueden, S. Saalfeld, B. Schmid, J. Y. Tinevez, D. J. White, V. Hartenstein, K. Eliceiri, P. Tomancak, A. Cardona, Fiji: An open-source platform for biological-image analysis. *Nat. Methods* **9**, 676–682 (2012).
85. C. Cirotti, S. Rizza, P. Giglio, N. Poerio, M. F. Allega, G. Claps, C. Pecorari, J. H. Lee, B. Benassi, D. Barila, C. Robert, J. S. Stamler, F. Cecconi, M. Fraziano, T. T. Paull, G. Filomeni, Redox activation of ATM enhances GSNOR translation to sustain mitophagy and tolerance to oxidative stress. *EMBO Rep.* **22**, e50500 (2021).
86. A. Schmidt, M. Eriksson, M. M. Shang, H. Weyd, J. Tegner, Comparative analysis of protocols to induce human CD4+Foxp3+ regulatory T cells by combinations of IL-2, TGF-beta, retinoic acid, rapamycin and butyrate. *PLOS ONE* **11**, e0148474 (2016).
87. S. Picelli, O. R. Faridani, A. K. Bjorklund, G. Winberg, S. Sagasser, R. Sandberg, Full-length RNA-seq from single cells using Smart-seq2. *Nat. Protoc.* **9**, 171–181 (2014).
88. E. Afgan, D. Baker, B. Batut, M. van den Beek, D. Bouvier, M. Cech, J. Chilton, D. Clements, N. Coraor, B. A. Gruning, A. Guerler, J. Hillman-Jackson, S. Hiltemann, V. Jalili, H. Rasche, N. Soranzo, J. Goecks, J. Taylor, A. Nekrutenko, D. Blankenberg, The Galaxy platform for accessible, reproducible and collaborative biomedical analyses: 2018 update. *Nucleic Acids Res.* **46**, W537–W544 (2018).
89. A. Kucukural, O. Yukselen, D. M. Ozata, M. J. Moore, M. Garber, DEBrowser: Interactive differential expression analysis and visualization tool for count data. *BMC Genomics* **20**, 6 (2019).
90. H. Heberle, G. V. Meirelles, F. R. da Silva, G. P. Telles, R. Minghim, InteractiVenn: A web-based tool for the analysis of sets through Venn diagrams. *BMC Bioinform.* **16**, 169 (2015).
91. G. Yu, Q. Y. He, ReactomePA: An R/Bioconductor package for reactome pathway analysis and visualization. *Mol. Biosyst.* **12**, 477–479 (2016).
92. M. Lerdrup, J. V. Johansen, S. Agrawal-Singh, K. Hansen, An interactive environment for agile analysis and visualization of ChIP-sequencing data. *Nat. Struct. Mol. Biol.* **23**, 349–357 (2016).

Acknowledgments
Funding: This work was supported by Lundbeck Foundation (R199-2015-2368, R210-2015-3372, and R291-2016-536), Danish Council for Independent Research–Medicine (DFF-4183-

00427 and 9039-00338), Danish MS Society, and Novo Nordisk Foundation, project grant no. NNF21OC0072256. **Author contributions:** S.I.-N. and S.M. conceived the study and designed experiments. S.R. and S.M. carried out the microscopy experiments. M.H. and L.M.R. prepared samples for RNA-seq and ChIP-seq and analyzed the data. S.M. and K.H. performed Seahorse, MTG, and TMRE experiments. J.Z., S.M. and J.M.-N. performed WB analysis. Y.L. and S.M. performed a reverse transcription qPCR experiment and in vitro suppression assay. K.H.K. provided FoxA1$^{fl/fl}$ mice. S.M. and S.I.-N. wrote the original draft. All authors took part in reviewing and editing the final manuscript. All authors read and accepted the manuscript. **Competing interests:** The authors declare that they have no competing interests. **Data and materials availability:** All data needed to evaluate the conclusions in the paper are present in the paper and/or the Supplementary Materials. Excel Files of RNA-seq and ChIP-seq data are available in the supplementary auxiliary files.

Submitted 19 July 2023
Accepted 20 November 2023
Published 20 December 2023
10.1126/sciadv.adj8442